

## Review Article

## Cretaceous (Maastrichtian) Vertisols of the Serra da Galga Member (Bauru Basin, Brazil): Implications for palaeoclimate and palaeoecology



Vithor Di Donato <sup>a,\*</sup>, Maurícius Nascimento Menezes <sup>a</sup>, Patrick Führ Dal' Bó <sup>a</sup>, Daniel Sedorko <sup>b</sup>, Jon J. Smith <sup>c</sup>, Leonardo Borghi <sup>a</sup>

<sup>a</sup> Laboratory of Sedimentary Geology (Lagesed), Department of Geology, Institute of Geosciences, Federal University of Rio de Janeiro, 21941-916 Rio de Janeiro, RJ, Brazil

<sup>b</sup> National Museum - UFRJ, Department of Geology and Paleontology, 20940040 Rio de Janeiro, RJ, Brazil

<sup>c</sup> Kansas Geological Survey, The University of Kansas, Lawrence, Kansas 66047-3724, USA

## ARTICLE INFO

Editor: Howard Falcon-Lang

## Keywords:

Serra da Galga Member  
Paleopedology  
Continental ichnology  
Beaconites  
Slickenside

## ABSTRACT

In this paper, we report the occurrence of Cretaceous (Maastrichtian) Vertisols from three profiles in the Serra da Galga Member (Marília Formation) of the Bauru Basin, Brazil, which developed as distributary fluvial deposits. Through integrated analysis of macroscopic and microscopic pedogenic features, clay mineralogy, whole-rock geochemistry, and ichnofossil assemblages, we assess the roles of climate, biota, and topography in shaping pedogenesis and organismal behavior under seasonal climatic regimes. The primary pedogenic processes identified include argilliturbation, clay translocation, calcification, and biological activity. Paleoclimatic reconstructions indicate mean annual precipitation ranging from 290 to 614 mm/year (mean:  $504 \pm 33$  mm/year) and mean annual temperature between  $10.6^{\circ}\text{C}$  and  $12.2^{\circ}\text{C}$  (mean:  $11.4 \pm 0.62^{\circ}\text{C}$ ). Köppen-based aridity indices suggest that all soil horizons formed under semiarid to subhumid conditions. The ichnoassemblages include invertebrate traces (*Taenidium*, *Skolithos*, and *Beaconites*) and plant-related structures (calcareous rhizocrusts, rhizohalos, and calcified bulbilous structures), exhibiting low to moderate bioturbation degree. The correlation between ichnofossil distribution, bioturbation intensity, geochemical data, and pedogenic characteristics suggests that the Vertisols developed under distinct seasonal climatic conditions. These soils displayed moderate drainage, characterized by short-term rises in the water table within the floodplain, followed by prolonged dry periods. Soil moisture availability played a crucial role in regulating biotic activity throughout these seasonal fluctuations. The results obtained not only enhance the understanding of pedogenetic and paleoecological processes during the Maastrichtian in the Bauru Basin but also provide a model for interpreting Vertisol formation in semiarid environments at mid-latitudes. Furthermore, they may provide a useful basis for global paleoclimate reconstructions.

## 1. Introduction

Soils form in response to environmental factors such as climate, parent material, biota, topography, and time (Jenny, 1941). Even subtle variations in these factors can lead significant changes in soil characteristics and properties (Retallack, 1997; Kraus, 1999). Among these factors, climate plays a pivotal role in regulating weathering processes by controlling temperature and water availability, which, in turn, influence soil distribution and biological diversity (Birkeland, 1999; Buol et al., 2003; Hembree and Nadon, 2011). In paleosols, in addition to

these formative factors, shallow and deep diagenetic processes influence the preservation of pedogenetic features. Despite these diagenetic alterations, the chemical composition of paleosols often remains largely intact, even under burial conditions (Mora et al., 1998). Consequently, geochemical analyses provide valuable insights into pedogenesis, the precipitation of pedogenic carbonates, and clay mineral formation (Sheldon et al., 2002; Retallack, 2001; Sheldon and Tabor, 2009; Tabor and Myers, 2015; Menezes et al., 2022). These geochemical signatures are also applied as paleoclimatic proxies, particularly for estimating quantitative parameters such as paleoprecipitation and

\* Corresponding author.

E-mail addresses: [vithordidonato@geologia.ufrj.br](mailto:vithordidonato@geologia.ufrj.br) (V. Di Donato), [m.nascimento@geologia.ufrj.br](mailto:m.nascimento@geologia.ufrj.br) (M.N. Menezes), [patrickdalbo@geologia.ufrj.br](mailto:patrickdalbo@geologia.ufrj.br) (P.F. Dal' Bó), [sedorko@mn.ufrj.br](mailto:sedorko@mn.ufrj.br) (D. Sedorko), [jjsmith@ku.edu](mailto:jjsmith@ku.edu) (J.J. Smith), [lborghi@geologia.ufrj.br](mailto:lborghi@geologia.ufrj.br) (L. Borghi).

paleotemperature (Sheldon et al., 2002; Nordt and Driese, 2010; Galagher and Sheldon, 2013).

Trace fossils preserved in paleosols provide key evidence of the paleobiota that once inhabited these ancient environments (Hasiotis, 2002). These organisms, whether permanent residents or transient visitors, directly influenced soil composition, density, drainage and chemistry, and thus played a central role in pedogenetic processes (Bardgett, 2005; Lavelle and Spain, 2001; Hembree and Nadon, 2011). In addition, paleoecological interactions in continental settings were strongly conditioned by factors such as substrate consistency, moisture content, nutrient availability, redox conditions, groundwater levels, seasonality, and the frequency of disturbance events (Hole, 1981; Buatois and Mángano, 2002; Hasiotis, 2002; Hembree and Nadon, 2011; Hembree and Blair, 2016; Sedorko et al., 2020, 2024, 2025; Goulart et al., 2025). Yet, despite their potential, the integration of paleosol proxies with ichnological analyses remains comparatively underdeveloped, especially in the Southern Hemisphere and notably within Brazilian sedimentary basins. Bridging this gap is essential, as trace fossils in paleosols represent a globally relevant but still underutilized archive for reconstructing paleoclimatic fluctuations, exposure durations, landscape evolution, atmospheric CO<sub>2</sub> dynamics, and the broader interplay of paleoenvironmental and paleoecological processes.

Vertisols are clay-rich soils characterized by pronounced shrink-swell behavior, shaped by multiple soil-forming factors including parent material, climate, topography, vegetation, and time. They typically develop under seasonal climatic regimes marked by periodic hydric stress or soil moisture deficits and are most commonly found in warm temperate to tropical regions (Coulombe et al., 1996a, 1996b). Vertisols generally occur in flat to gently sloping lowland settings and are frequently associated with native vegetation such as grasslands and savannas (Dudal, 1965; Probert et al., 1987). These soils are distinguished by high concentrations of expansive clay minerals, primarily smectite, which may form in situ through neoformation or be inherited from the parent material (Dudal, 1965; Ahmad, 1983; Probert et al., 1987; Coulombe et al., 1996a, 1996b). Diagnostic features of Vertisols include pedogenic slickensides, gilgai microtopography, and a distinctive sepic-plasmic clay microfabric, hallmarks of their dynamic physical evolution (Coulombe et al., 1996a, 1996b; Driese and Ober, 2005).

The study of Vertisols through geological time has been more extensively pursued in the Northern Hemisphere (e.g., Caudill et al., 1996; Driese et al., 2000; Nordt and Driese, 2010). In contrast, investigations in the Southern Hemisphere remain relatively limited, with most occurrences concentrated in Argentina and Brazil (Dal' Bó and Basilici, 2010; Varela et al., 2017; Soares et al., 2021; Lizzoli et al., 2025; Raigemborn et al., 2025). In Argentina, Cretaceous Vertisols are particularly well developed in the Patagonian region and were generated under temperate to warm-temperate, humid to subhumid climatic conditions with marked rainfall seasonality. Meanwhile, Vertisols of the Marília Formation (Bauru Basin) in Brazil often display calcic horizons and are associated with seasonal semi-arid to subhumid climates, reflecting their occurrence within the southern hot arid belt. However, unlike in Argentina, Cretaceous Vertisols in Brazil have received more attention in paleoenvironmental and stratigraphic studies than in pedological and paleoclimatological research. As a result, aspects related to pedogenic processes and the influence of climatic and biological controls have often been overlooked or underexplored.

In this context, the lack of detailed studies on fossil Vertisols in the Southern Hemisphere constitutes a significant gap in paleoclimatic and paleoecological reconstructions at mid-latitudes, especially during climatic transition intervals such as the Maastrichtian. By integrating pedological, mineralogical, geochemical, and ichnological analyses, this study proposes a process-based model applicable to other semi-arid systems, offering valuable insights into environmental heterogeneity, hydrological dynamics, and biological interactions through geological time. In fluvial floodplains, trace fossils encapsulate the interaction of soils, flooding, and biotic activity, offering a globally relevant archive of

ecosystem resilience and climatic response (Buatois and Mángano, 2002). Moreover, the methodological advances regarding the application of geochemical indices in Vertisols contribute to the refinement of global proxies for precipitation and temperature, with implications that go beyond the regional scale and directly engage with current discussions on landscape evolution in arid and semi-arid environments.

## 2. Geological setting

The Cretaceous Bauru Basin, dating from the Aptian to Maastrichtian age, occurs in areas from western Paraná, western São Paulo, eastern Mato Grosso do Sul, southern Goiás, and western Minas Gerais, totaling approximately 370,000 km<sup>2</sup> in area. It has an elliptical shape, with its long axis oriented in a northeasterly direction (Batezelli, 2015). Its boundaries are defined by the Alto Paranaíba Uplift (NE), the Goiás Alkaline Province (N), the Rondonópolis Uplift (NW), the Asunción Arch (SW), and the Serra do Mar Range (E; Batezelli, 2003). The basin developed within the South American Platform following the deposition of basalts from the Serra Geral Formation (Valanginian-Hauterivian) during the breakup of the Gondwana supercontinent, driven by thermo-mechanical subsidence processes (Fernandes and Coimbra, 1996; Thiede and Vasconcelos, 2010; Batezelli, 2015).

The sedimentary thickness reaches up to 300 m, predominantly characterized by sandy and muddy deposits, formed under a sub-humid to arid climate during the Coniacian to Maastrichtian period (Dal' Bó et al., 2009; Batezelli, 2015; Menezes et al., 2022). The stratigraphic framework of the basin is complex due to their vast extent, unclear biostratigraphic and geochronologic data, and the high rates of pedogenic processes, which have formed thick successions of paleosols that make up to 60 % of the sedimentary record of the basin (Basilici et al., 2016). The sedimentary deposits of the Bauru Basin have been subdivided into two lithostratigraphic units: the Caiuá and Bauru groups. The Bauru Group is stratigraphically represented by the Araçatuba, Adamantina, Uberaba, and Marília formations (e.g., Batezelli, 2015).

The Marília Formation was deposited during the Maastrichtian, as evidenced by the assemblage of Late Cretaceous fossils, including conchostracans, ostracods, charophytes, sauropods, theropods, crocodylomorphs, and pterosaurs (Dias-Brito et al., 2001; Gobbo-Rodrigues, 2001; Santucci and Bertini, 2001; Candeiro and Rich, 2010; Carvalho et al., 2010; Martinelli et al., 2011; Kellner et al., 2019). Its lower stratigraphic boundary is in contact with the Adamantina Formation (in São Paulo State) and the Uberaba Formation (in the Triângulo Mineiro region), while its upper limit coincides with the Cretaceous–Paleogene boundary (Dias-Brito et al., 2001; Zalán and Oliveira, 2005). Above the Marília Formation, the Sul-Americana (in the southeastern region) or Pratinha (in the Triângulo Mineiro region) Surface reveals evidence of a generalized erosional surface formed by the reactivation of pre-existing tectonic structures, resulting in an uplift that altered the topography of the basin boundaries. This regional surface, which developed between 93 and 60 million years ago, has been dated to 65.65 ± 0.05 million years (Riccomini et al., 2004; Dias et al., 2018), attesting the chronostratigraphic position of this unit. The Marília Formation consists of three members: Ponte Alta, Serra da Galga, and Echaporã, with the Serra da Galga Member being the focus of the present study.

The Serra da Galga Member is approximately 110 m-thick, presenting sedimentary deposits of polymictic conglomerates, conglomeratic sandstone, and mudstone interbedded with paleosols and pedogenic calcretes. This member is interpreted as deposits from the proximal to medial zones of an ancient distributive fluvial system (Dal' Bó et al., 2010; Batezelli et al., 2019). Paleosols in the Serra da Galga Member comprise two soil orders: Entisols and Vertisols, characterized by distinct horizons (calcic, argillic, and vertic), carbonate nodule concentrations, blocky and wedge-shaped structures, slickensides, pedogenic minerals, and continental trace fossils (Mineiro and Santucci, 2018; Dal' Bó et al., 2019; Rodrigues et al., 2019). The paleosol trace fossils have been described as dominated by rhizoliths, *Skolithos* isp.,

and *Taenidium barretti*, indicating an overall low ichnodiversity and limited distribution (Mineiro and Santucci, 2018; Rodrigues et al., 2019; Nascimento et al., 2022).

### 3. Materials and methods

The studied outcrop is located along the road BR 050, km 153, between the municipalities of Uberaba and Uberlândia in the Triângulo Mineiro region, state of Minas Gerais, Brazil (Fig. 1). The outcrop is 20 m high and 70 m long, exposing sedimentary rocks and paleosols of the Serra da Galga Member. Three vertically stacked paleosol profiles, 0.75 m to 1.32 m thick, were surveyed and described with respect to lithology, macro- and micromorphological soil characteristics, geochemistry, and ichnofossils. Paleosol recognition followed the criteria outlined by Catt (1990) and Retallack (2001), while individual horizons were described according to Schoeneberger et al. (2012) and classified using the US Soil Taxonomy (Soil Survey Staff, 1999).

The identification of trace fossils involved a comparative methodology with literature data. Initially, the ichnotaxobases proposed by Bromley (1996) were consulted for morphological descriptions and taxonomic classification of ichnofossils. The toponomic classification of ichnofossils was conducted according to Seilacher (1964), while the distribution followed the precepts of Gingras et al. (2011). Additionally, the ichnological relationship with the water table was based on Retallack (2001), Kraus and Hasiotis (2006), and Hasiotis et al. (2007). Finally, this study addressed the quantification of bioturbation intensity

as proposed by Reineck (1963), where the degree values range from 0 to 6, with 0 representing the absence of bioturbation and 6 indicating a rock completely obliterated by biogenic activity.

A total of 12 oriented and representative paleosol samples were systematically collected for micromorphological and geochemical analysis. Detailed analysis of these 12 thin sections, impregnated with blue epoxy under vacuum, was conducted using a Zeiss Axio Imager petrographic microscope. Micromorphological observations followed the descriptive methods outlined by Bullock et al. (1985) and Stoops et al. (2010). Carbonates were identified using a potassium ferricyanide and Alizarin Red-S solution (Dickson, 1965). The mineralogical composition of the paleosol horizons was determined through X-Ray Diffractometry (XRD). For this purpose, ten oriented samples with particle sizes <2 µm were subjected to air-drying, glycol solvation, and heating to 550 °C. XRD patterns were obtained using a Bruker D8 Advance Eco diffractometer equipped with a CuK $\alpha$  radiation source ( $\lambda = 1.5418 \text{ \AA}$ ) and operated in a 0-0 configuration. Analyses were conducted at CETEM (Centro de Tecnologia Mineral, Rio de Janeiro). Diffractograms were generated using Bruker's DiffracPlus software and interpreted through qualitative mineralogical analysis by comparison with the International Centre for Diffraction Data (ICDD; PDF-04) database. Scanning Electron Microscopy (SEM) analyses were performed on both natural and thin section, etched samples following the protocol of Folk (1993). Imaging was conducted using two instruments: a FEI Quanta 400 operating in low-vacuum mode at 20 kV with a Backscattered Electron Detector (BSED) and no coating, and a Hitachi TM3030Plus

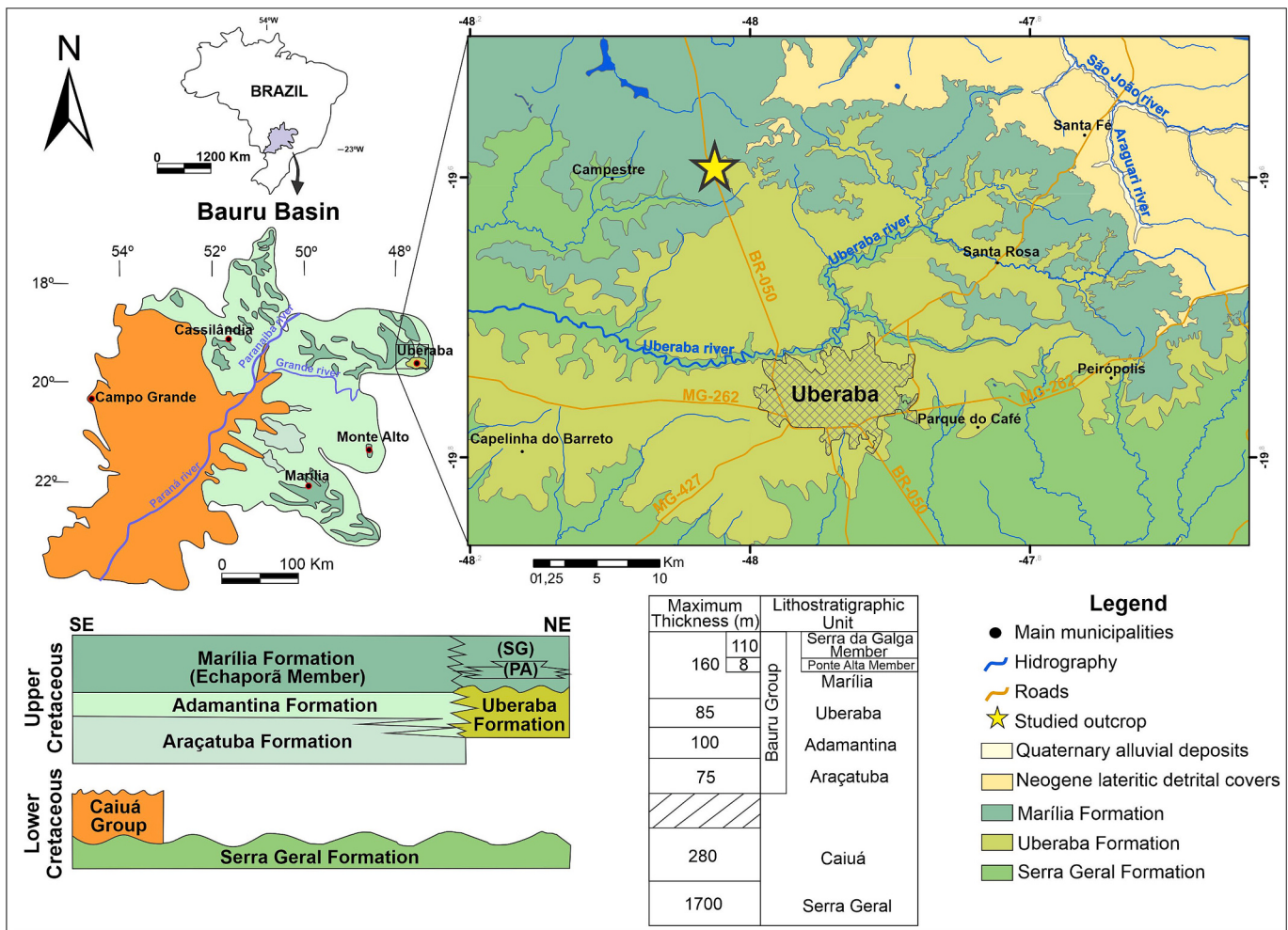


Fig. 1. Geological and stratigraphic features of the study area (Modified from Batezelli, 2015; Soares et al., 2017). PA: Ponte Alta Member; SG: Serra da Galga Member.

operating in high-vacuum mode at 15 kV with a Secondary Electron Detector (SED) and gold coating.

To determine the geochemistry of the main oxides, 10 Vertisol samples were prepared at the Centro de Tecnologia Mineral (CETEM, Rio de Janeiro) through drying and pulverization. Subsequently, the samples underwent lithium borate fusion and were analyzed using an X-Ray Fluorescence Spectrometer (XRF). The results, presented as weight percentages of oxides (Table 1), were then normalized to molecular weight to facilitate comparisons of oxide weight proportions both within and between units, following the methodology outlined by Retallack (2001). The values were used to calculate molecular weathering ratios, representing the effects of  $\sum \text{Bases}/\text{Al}$ , oxidation, clay content, salinization, calcification and calcium–magnesium weathering index (CALMAG; Retallack, 2001; Nordt and Driese, 2010). Mean annual precipitation (MAP) for each horizon was calculated using the calcium–magnesium weathering index (CALMAG) and chemical index of alteration without potassium (CIA—K), which carries a standard error of  $\pm 108$  mm (Nordt and Driese, 2010). Mean annual temperature (MAT) was estimated using paleosol weathering index proxy (PWI), in which the limited of temperature range is between 8° and 36 °C (Gallagher and Sheldon, 2013), and standard error of  $\pm 0.23$  °C (Table 2).

#### 4. Results

The studied vertical succession consists of three well-defined stratigraphic intervals: the base is characterized by phreatic calcrite (Ponte Alta Member), followed by fluvial deposits in the middle (Serra da Galga Member), and Cenozoic deposits at the top. The outcrop (Fig. 2A) features conglomeratic sandstones and fine to coarse-grained sandstones, which are poorly to moderately sorted and composed of pebble- to granule-sized clasts, as well as coarse- to medium-grained sand. These lithoclasts are subangular to sub-rounded and include quartz, lithic fragments, and feldspar. The sedimentary structures described are planar-parallel and cross-lamination, as well as low-angle cross-stratification. The deposits form tabular, isolated, or amalgamated bodies, characterized by basal erosive surfaces and flat tops, interbedded with floodplain deposits where the paleosols are found.

##### 4.1. Vertisols profile description

Profile 1 (Fig. 2B), with a thickness of 93 cm, is organized into four horizons, sequenced as Bssk, Bssk2, Bss, and C. The base is marked by gradual contact with conglomeratic sandstone, while the top of the profile displays an erosional surface. The transition between the horizons is gradual and undulating, with smooth or wavy topography (Fig. 3A). The texture is loamy-sand in vertic (Bssk and Bss) horizons, and sandy in C horizon. The paleosol colors are light reddish brown (2.5YR 7/4) in the B horizons and light reddish brown (2.5YR 6/4) in the C horizon. The Bss horizon presents wedge-shaped pedogenic structures with diameters ranging from 1 to 4 cm, which can be subdivided into angular blocks of 10–70 mm. Redoximorphic features, such as redox depletion and redox concentration, are also recognized in this horizon,

**Table 2**  
Molecular weathering ratio and paleoclimate proxy equations.

Molecular Weathering Index	Equation	Pedogenic Process	Climofunctions
$\Sigma \text{Bases} / \text{Al}$	$(\text{CaO} + \text{MgO} + \text{Na}_2\text{O} + \text{K}_2\text{O}) / \text{Al}_2\text{O}_3$	Hidrolysis	–
Calcification	$(\text{CaO} + \text{MgO}) / \text{Al}_2\text{O}_3$	Calcification	–
Clay content	$\text{Al}_2\text{O}_3/\text{SiO}_2$	Hidrolysis	–
Salinization	$(\text{Na}_2\text{O} + \text{K}_2\text{O}) / \text{Al}_2\text{O}_3$	Salinization	–
Oxidation	$(\text{Fe}_2\text{O}_3 + \text{MnO}) / \text{Al}_2\text{O}_3$	Oxidation	–
CIA-K	$(\text{Al}_2\text{O}_3 / (\text{Al}_2\text{O}_3 + \text{CaO} + \text{Na}_2\text{O})) \times 100$ $[(4,2^*\text{Na}) + (1,66^*\text{Mg}) + (5,54^*\text{K}) + (2,05^*\text{Ca})] \times 100$	Clay content	
PWI		Hidrolysis	$\text{MAT} = -2,74 * \ln(\text{PWI}) + 21,39$
CALMAG	$\text{Al}_2\text{O}_3 / (\text{Al}_2\text{O}_3 + \text{CaO} + \text{MgO}) \times 100$	Clay content	$\text{MAP} (\text{mm/yr}) = 22,69 * \text{CALMAG} - 435,8$

covering 40 % of the horizon surface. Distinct iron depletions along macropores, ranging in size from medium to coarse (0.5–15 cm in diameter), occupy 25 % of the horizon. Fe-nodule concentrations, with diameters ranging from 1 mm to 6 mm, are distributed across 15 % of the horizon. Another concentration feature is pore linings, occurring along root channels and invertebrate trace fossils, with colors varying from gray to red and dark red. The Bssk horizon exhibits fine to medium, subangular to angular blocky peds, varying in size from 2 to 5 cm. Submillimeter-thick, sub-horizontal laminae with two or three bifurcation directions, ranging from 0.5 to 1 mm in thickness and extending laterally up to 1 m, composed of sparry calcite, occupy 20 % of the horizon (Fig. 3B). Fine calcium carbonate nodules, varying from 5 mm to 1 cm in diameter, are disseminated throughout the horizon. All vertic horizons exhibit gray-green slickensides with centimeter-scale, convex-concave slip surfaces, and a striking pattern around 135/18. The trace fossil assemblage is composed of calcareous rhizoconcretions, rhizoholas, *Skolithos*, *Taeniidium* and *Beaconites*, with low to moderate ichnodiversity and bioturbation degree of 2–3, reaching 4 in one bedding-plane.

Profile 2 (Fig. 2C) is 60 cm-thick, and is organized into three horizons, sequenced as Bssk, Bssk2, and BCk. The base is marked by a gradual contact with fine to medium-grained sandstone, and the top features an erosional surface. The transition between the horizons is clear to undulating, with smooth or wavy topography. The texture is loamy-sand in the vertic horizons and conglomeratic sandy in the BCk horizon. The colors of the horizons are light greenish-gray (5 GY 7/1) in the vertic horizons and pinkish-white (7.5 YR 8/2) in the BCk horizon. The pedogenic structures in the vertic horizons are well-formed wedge-shaped structures (Fig. 3C) that can fracture into angular blocky peds, with diameters ranging from 4 to 9 cm. The planes separating the peds are marked by gray-green slickensides, 6 to 15 cm long, with convex-

**Table 1**  
Major elements from Serra da Galga Vertisols, reported as oxide percentages.

Profile	Horizons	SiO <sub>2</sub>	Al <sub>2</sub> O <sub>3</sub>	Fe <sub>2</sub> O <sub>3</sub> (T)	MnO	MgO	CaO	Na <sub>2</sub> O	K <sub>2</sub> O	TiO <sub>2</sub>	P <sub>2</sub> O <sub>5</sub>
1	Bssk	52.8	7.3	3.9	0.08	1.8	6.0	0.12	3.0	1.1	0.62
	Bssk2	62.4	10.5	5.8	0.15	2.5	4.1	0.16	4.2	1.4	0.53
	Bss	63.6	10.5	5.7	0.14	2.5	4.2	0.08	4.1	1.4	0.46
	C	69.7	11.0	6.3	0.07	2.6	2.8	0.08	4.2	1.7	0.36
2	Bssk	81.1	6.3	3.7	0.16	1.5	2.9	0.08	2.7	1.8	0.23
	Bssk2	77.6	5.9	3.3	0.03	1.3	2.0	0.08	2.5	1.8	0.23
	BCk	77.0	6.1	3.5	0.08	1.3	2.2	0.08	2.6	1.8	0.19
3	Bss	65.5	9.3	3.9	0.05	1.9	5.0	0.08	3.5	0.97	0.23
	Bssk	60.6	8.4	3.5	0.05	1.8	5.2	0.08	3.1	0.95	0.20
	BCk	64.9	9.5	4.3	0.06	2.1	4.8	0.08	3.6	1.0	0.23

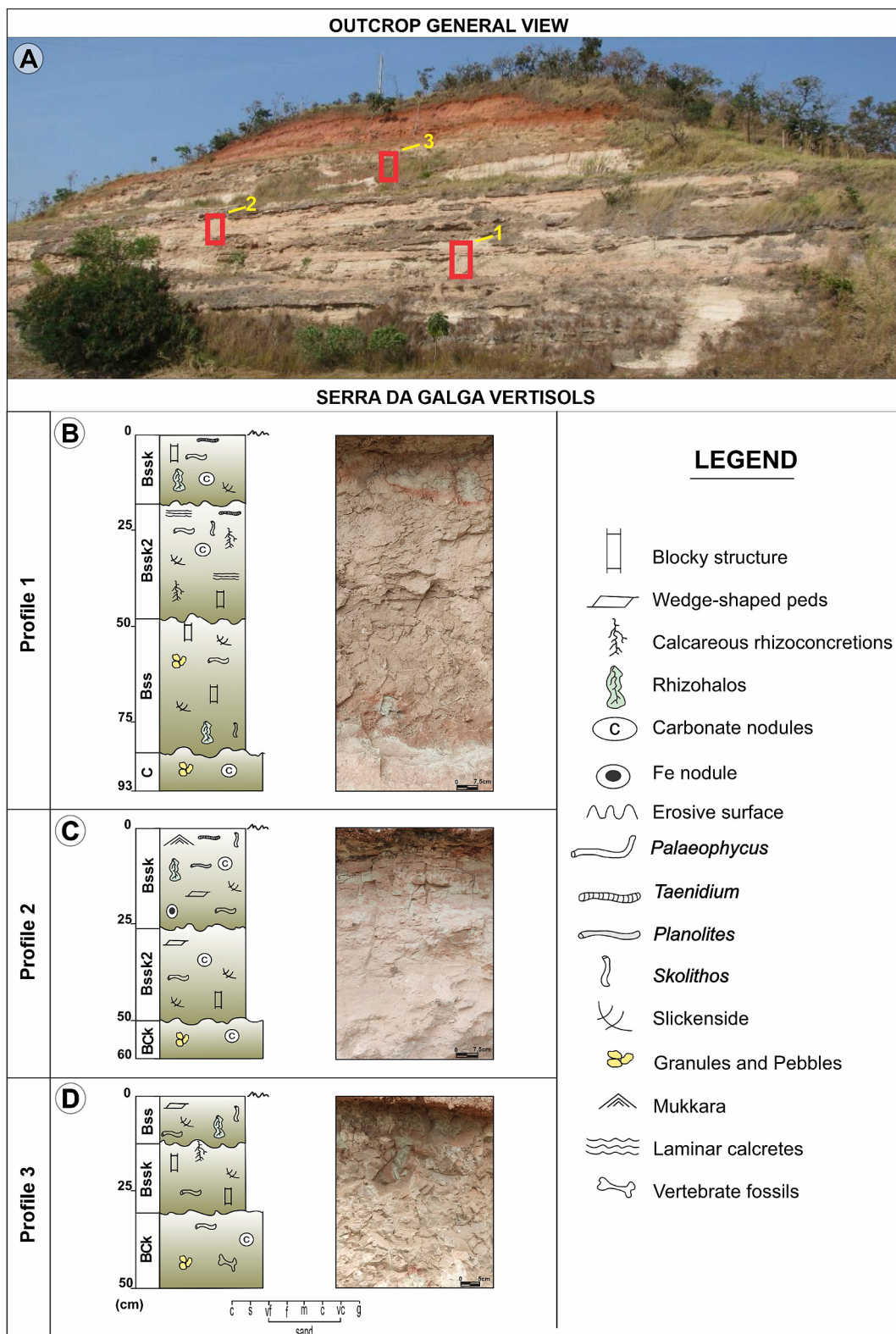


**Fig. 2.** Drafted geologic sections and outcrop photographs with position of described profiles in the Serra da Galga Member.

concave slip surfaces (Fig. 3D) and an average striking pattern of 229/18 and 073/16 (Fig. 4). Coupled with clay deformation, the variation in horizon morphology, expressed as pseudo-anticlines (micro-highs) and swales (micro-lows), forms a mukkara structure (Fig. 3E). This micro-relief exhibits highs of approximately 10 cm and lows of up to 15 cm, with flank slopes varying from 073/16 (F1) to 229/18 (F2) within the

Bssk horizon (Fig. 4). The overall ground slope at the Profile 2 Vertisol outcrop was measured using a field clinometer and compass, revealing a consistent dip of approximately ~5° toward 222° (SW) across the Bssk horizon. Measurements were taken at 5-m intervals, with an average elevation difference of 0.42 m between points. Additionally, small vertical cracks filled with very fine sand are present at the top of the micro-

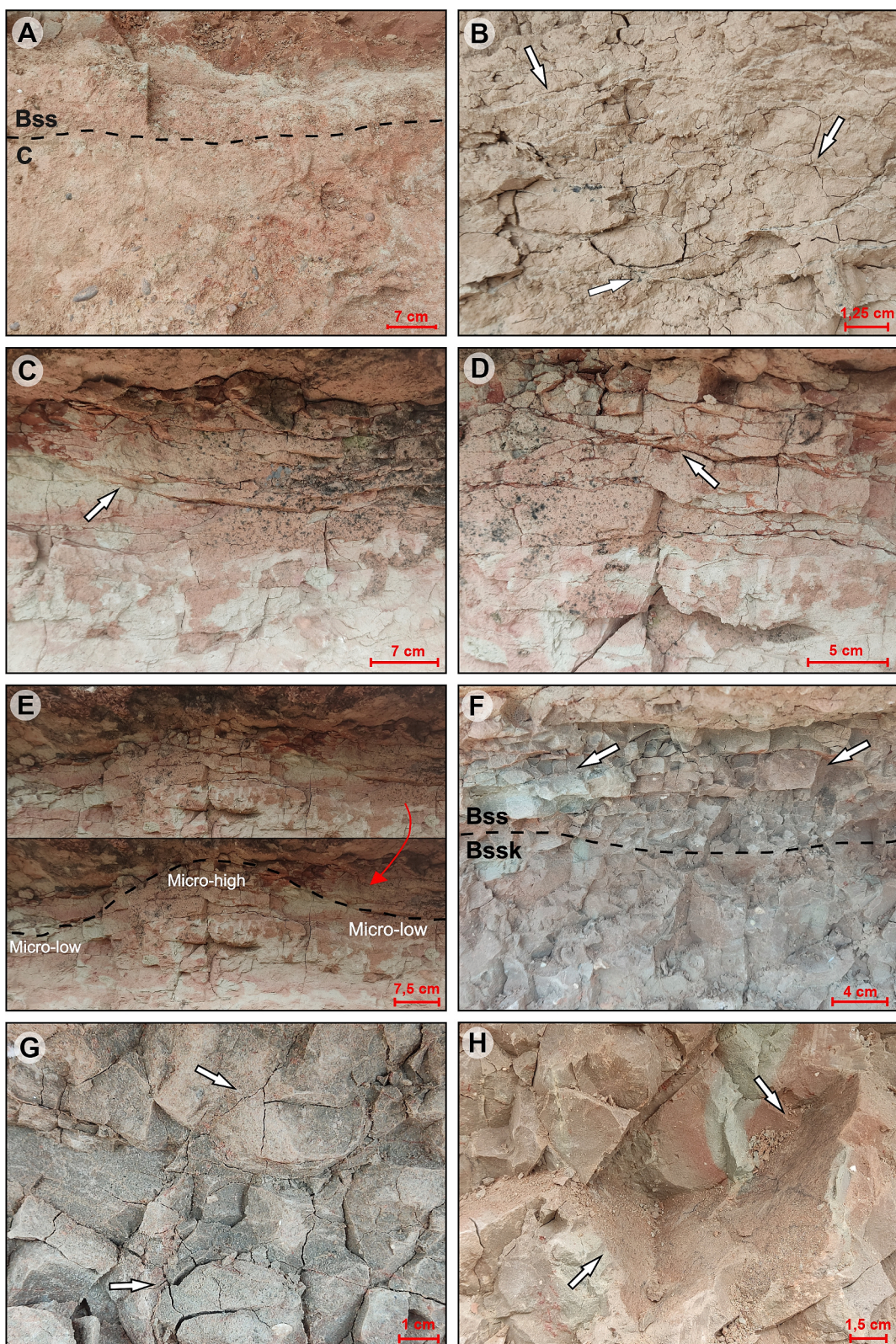


**Fig. 3.** Macroscopic Features of Serra da Galga Member Vertisols. (A) Boundary between the Bssk horizon and the C horizon, marked by black dashed lines. (B) Laminated structures, indicated by white arrows, scattered in the Bssk horizon and oriented subparallel. (C) Wedge-shaped peds, highlighted by the white arrow. (D) Clay films between peds, commonly filling slickenside surfaces, indicated by white arrows. (E) Mukkara-type microrelief, outlined by the black dashed line, showing the highs and lows of the morphology. (F) Boundary between Bss and Bss<sub>2</sub> horizons, featuring redoxmorphic features and block structures concentrated in the upper part of the profile, indicated by white arrows. (G) Block-shaped peds, highlighted by the white arrow. (H) Slickenside planes marked by striations, highlighted by white arrows.

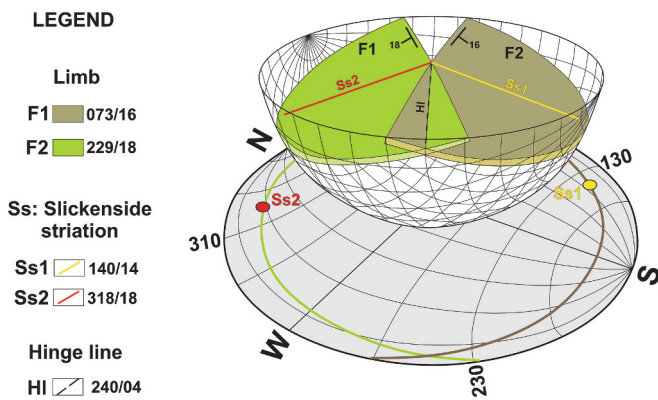


Fig. 4. Stereographic projection of slickenside and pseudoanticlinal attitudes.

highs. In the swales, the vertic horizons show iron oxide and calcium carbonate nodule concentrations of less than 10 %. Redoximorphic features of depletion and concentration are associated with pore linings along root channels and invertebrate ichnofossils, covering 10 to 30 % of the vertic horizon surface. In the BCk horizon, the nodules make up 3 % of the horizon's surface, with diameters varying from 0.5 to 2 cm. This horizon is characterized by limited pedogenic structure development and a reduced concentration of carbonate nodules. The trace fossil assemblage from the Profile 2 is composed of calcareous rhizoconcretions, rhizohalos, *Taenidium* and *Skolithos* with low bioturbation degree (1–2).

Profile 3 (Fig. 2D), with a thickness of 75 cm, is organized into three horizons, sequenced as Bss, Bssk and BCk. The base presents a gradual contact with medium sandstone, and the top shows an erosional surface. The transitions between the horizons are clear and undulating, with smooth or wavy topography (Fig. 3F). The texture is loamy-sand in the vertic horizons (Bss and Bssk), with a greenish-gray color (5G 6/1), and richer in sand in the BCk horizon, with a greenish-gray color (10 Y 6/1). The pedogenic structures in the vertic horizons exhibit small wedge-shaped and block structures (Fig. 3G), with lengths of less than 8 cm, and fine to medium angular blocky peds, varying in diameter from 1 to 5 cm. Redoximorphic features of depletion and concentration are associated with root channels. The gray-green slickensides, 4 to 10 cm long, consist of convex-concave slip surfaces (Fig. 3H), with a striking average pattern of 200/11 and 088/18. The BCk horizon, however, does not display any visible pedogenic structures or sedimentary evidence of the parent material. Calcium carbonate nodules, varying from 1 to 4 cm in diameter, are disseminated throughout the horizon. The trace fossil assemblage from Profile 3 includes calcareous rhizoconcretions, and *Skolithos*, with low bioturbation degree (1–2).

#### 4.2. Vertisols mineralogy and micromorphology features

The mineral assembly was determined based on petrographic descriptions and XRD analyses. The main constituents of the Vertisol profiles are mono- and polycrystalline quartz, feldspars (orthoclase and microcline), anatase, pyrite, mica (muscovite and biotite), nontronite, montmorillonite, iron oxides and sepiolite (Fig. 5). Within the vertic horizons (Bss and Bssk), the mineral distribution includes quartz (40 % - 64 %), calcite and magnesian calcite (4 % - 18 %), potassium feldspar (microcline; 20 % - 27 %), clays (10 % - 18 %), siderite (0.01 % - 0.2 %), and other accessory minerals (1 % - 2 %). The clay content is predominantly smectite (nontronite and montmorillonite), varying from 52 % to 72 %. Scanning electron microscopy (SEM) reveals that smectite exhibits a characteristic honeycomb habit, that is, a three-dimensional cellular lattice defined by discrete pore spaces. The lattice walls, measuring 0.1–0.5 µm in thickness, enclose polygonal pores or form in situ on feldspar grains and are composed of clay platelets joined predominantly by face-to-face and face-to-edge contacts (Fig. 6A, B). Smectite flakes

form thin coatings on grain surfaces, fill intergranular pores, and line some micro-fractures (Fig. 6G). Mica is the second most abundant clay mineral, comprising 12 % to 40 % of the clay mineral content. Sepiolite is present in the second and third profiles, varying between 14 % and 27 %, respectively. Furthermore, hematite and siderite nodules, ranging from 2 to 4 mm in diameter and displaying red or dark red colors, are common within the matrices and in the color zones of rhizohalos.

Twelve representative thin sections of the vertic horizons (Bss and Bssk) were described based on aspects of pedality, coarse/fine (c/f) ratio, b-fabric, clay coatings, pedogenic calcium carbonate, and biogenic structures. The horizons exhibit weakly to moderately developed pedality and enaulic c/f related distribution. The coarse material primarily consists of quartz, feldspar, and lithic fragments, which are medium to coarse-grained sand, moderately to poorly sorted, and range from subangular to subrounded in shape. The clasts show a preferential orientation associated with slickenside plane surfaces (Fig. 7A, B). Alteration of lithic fragments, K-feldspar and plagioclase (Fig. 6E, F) varies from 1 (2.5 % - 25 %) to 2 (25 % - 75 %). The fine material is composed of pedogenic clay minerals and exhibits parallel striated (Fig. 6D), speckled, crystallitic, granostriated, and porestriated b-fabrics. Clay coatings are observed with capping and link capping morphologies (Fig. 6C, 7C), oriented parallel to the ped surfaces. The pedogenic structures are angular to subangular blocks (Fig. 7D), varying in diameter from 4 to 8 mm, with simple to complex voids associated. Pedogenic carbonates occur as micrite or sparry calcite, infilling laminar structures and concentrating adjacent to rhizoliths (Fig. 7E, F), or as spherulites measuring 200–500 µm in diameter. These spherulites, typically associated with biogenic structures, consist of crystals displaying a radial fibrous fabric with straight to undulatory extinction (Fig. 6H). Carbonate nodules, ranging from 2 to 6 mm in diameter, exhibit spherical to prolate shapes and are composed of an inequigranular coarse mosaic with nonplanar intercrystalline boundaries (Fig. 7G). These nodules are found in the Bssk horizons and account for approximately 25 % of the thin section, often engulfing or overgrowing both coarse and fine matrix components. Iron is present as nodules and concretions, 1–4 mm in diameter (Fig. 7H).

#### 4.3. Ichnology content

##### 4.3.1. Rhizoliths

Calcareous rhizoconcretions (Fig. 8A, B, C) are vertically to subvertically oriented and exhibit downward or horizontal branching patterns with bifurcations of variable thickness. These features are composed of white to gray calcite, ranging in texture from powdery to solid, and vary in size from 1 to 15 cm in length and 0.2 to 6 cm in diameter. Occasionally, calcified rhizospheres, interpreted as bulbous plant root structures, are present (Fig. 8C). These appear as spherical to subspherical features, reaching up to 15 cm in diameter and often associated with horizontal to subhorizontal sparry calcite laminar structures, which range from 0.2 to 1 cm in thickness. The rhizoconcretions are abundant in the first and second profiles, decreasing in distribution in the third profile. Rhizohalos (Fig. 8D, E) occur as circular to subcircular forms, individual structures ranging from 2 to 15 cm in diameter, with two edges showing different colors: the inner part has a light greenish-gray (5GY 7/1), while the outer rim is red (10R 5/8). Occasional diffuse carbonate concretions are present in the inner portions.

##### 4.3.2. Invertebrate trace fossils

The ichnofossils of invertebrates in the studied paleosols present three morphologies. The first is characterized as actively filled burrows with internal meniscate filling. These burrows are horizontally to subvertically oriented, cylindrical, sinuous or slightly arched, unbranched, and exhibit well-defined walls. They range from 3 to 8 cm in length and 0.5 to 1.5 cm in diameter, with an average diameter of 0.8 cm. The backfilled sediment within these burrows is composed of material

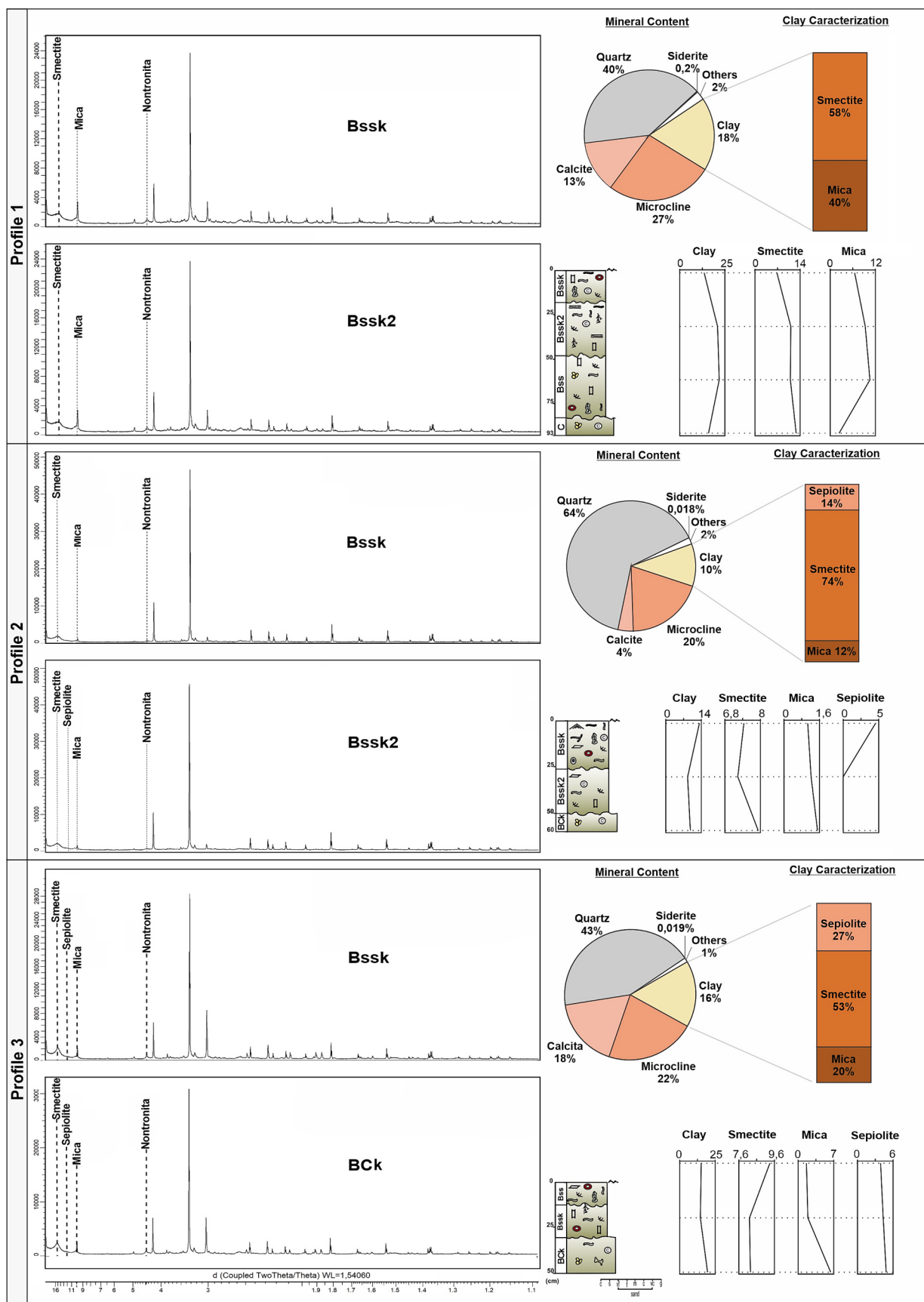


**Fig. 5.** Mineral Content of Serra da Galga Member Vertisols, with clay mineral identification by XRD, showing the percentage of mineral content and the distribution of clay minerals along of the Profiles.

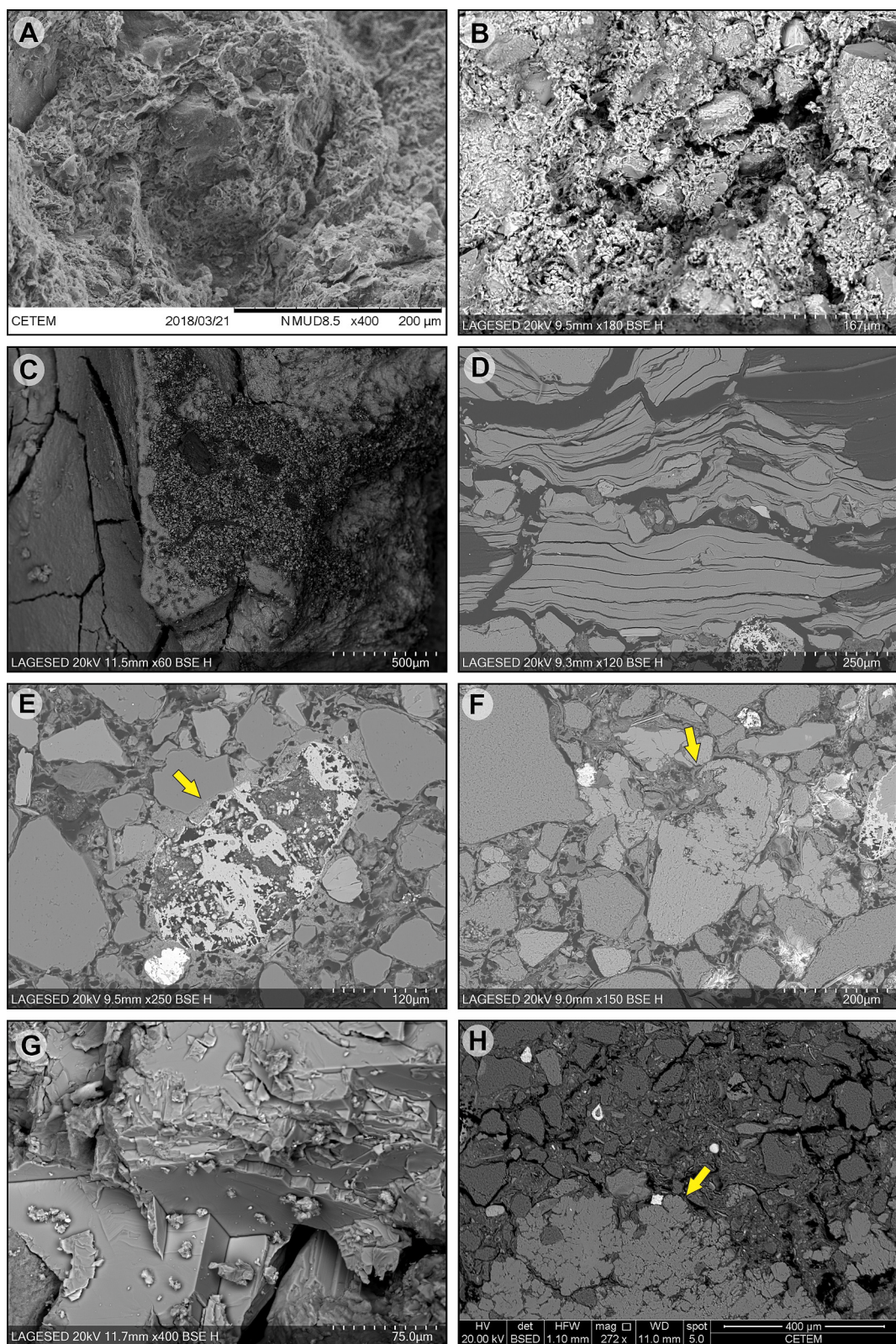


**Fig. 6.** SEM image of Serra da Galga Member Vertisols. (A) Honeycomb structure of smectite. (B) Honeycomb structure of smectite in Bss horizon. (C) Detrital clay capping peds in the Bss horizon. (D) Clay concentration oriented along the friction plane in the Bss horizon. (E) Carbonate coating highlighted by the yellow arrow, in Bssk horizon. (F) Autogenic clay formed by mineral weathering. (G) Cornflake structure of smectite above calcite grain. (H) Spherulite highlighted by the yellow arrow, in Bssk horizon. (For interpretation of the references to color in this figure legend, the reader is referred to the web version of this article.)

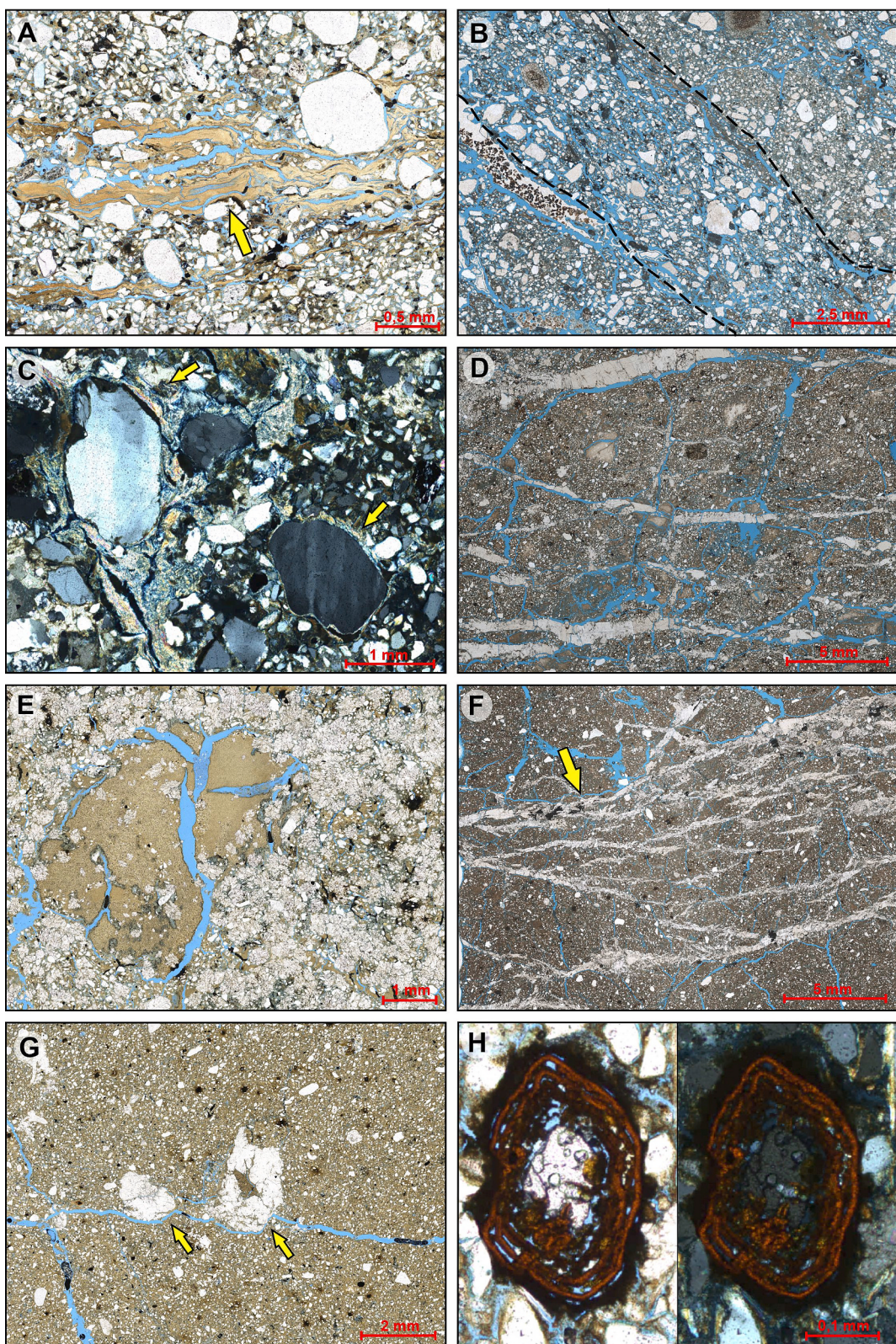


**Fig. 7.** Micromorphological and Mineralogical Characteristics of Serra da Galga Member Vertisols. (A) Clay concentration oriented along the friction plane (slickensides) in the Bss horizon, highlighted by the yellow arrow, under parallel nicols. (B) Alignment of grains and clays along deformation surfaces, outlined by the black dashed line, under parallel nicols. The arrows indicate the orientation. (C) Quartz grains surrounded by clay and carbonate coatings, under crossed nicols. (D) Subangular blocks separated by planar voids, under parallel nicols. (E) Bssk horizon showing spherulites, under parallel nicols. (F) Laminar Bssk horizon, under crossed nicols. (G) Carbonate nodules, highlighted by red arrows, under parallel nicols. (H) Iron concretions, observed under parallel nicols (left) and crossed nicols (right). (For interpretation of the references to color in this figure legend, the reader is referred to the web version of this article.)

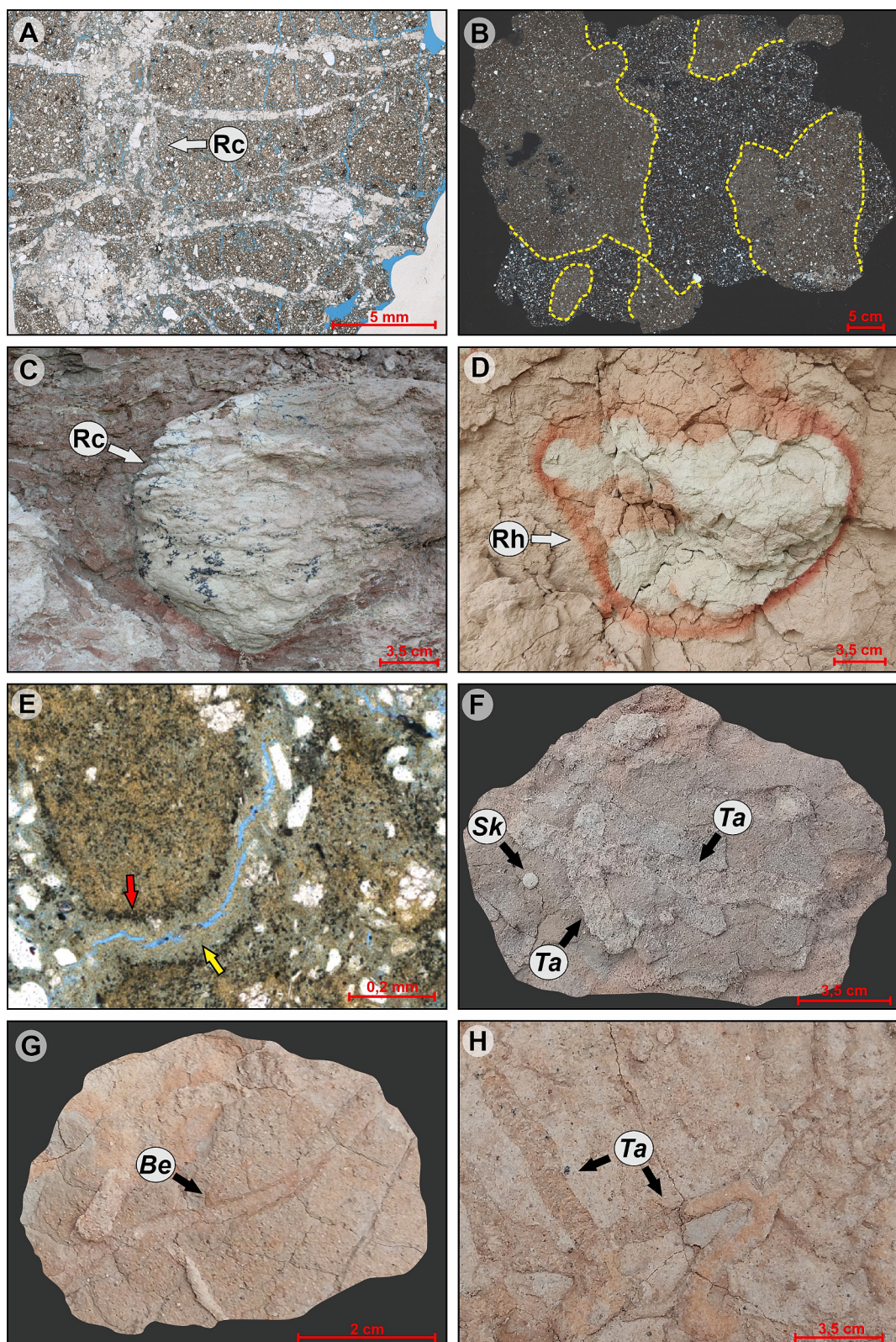


**Fig. 8.** Ichnological features of Serra da Galga Member Vertisols, predominantly present in Profile 1. (A) Laminar structure and rhizoconcretion in the Bssk horizon, under parallel nicols. (B) Transversal section of a rhizoconcretion, outlined by yellow dashed lines, in thin section, under crossed nicols. (C) rhizoconcretion characterized as a bulbous structure (calcified rhizosphere) within a predominantly clayey-sandy matrix. (D) Rhizohalo (Rh) with a subcircular morphology, exhibiting a whitish interior and a reddish ring at the edges. (E) Rhizohalo with manganese oxide and siderite (oxidized zone), highlighted by the red arrow, under parallel nicols, and a calcified inner portion (depletion zone), highlighted by the yellow arrow, under parallel nicols. (F) Sample with a superficial clay film, containing ichnofossils *Beaconites* isp. and *Skolithos* isp. (G) Sample showing the presence of *Beaconites* isp. (H) *Beaconites* isp. in a sample from the Bss horizon, with clearly visible menisci. (For interpretation of the references to color in this figure legend, the reader is referred to the web version of this article.)

similar to the surrounding matrix and is often organized into distinct meniscated packets, characterized by uniform spacing and thickness. This morphology is attributed to the ichnotaxon *Beaconites* isp. Vialov, 1962 (Fig. 8G). In contrast, similar structures lacking wall linings, comprising variable, oriented, straight, sinuous, or curved simple cylindrical burrows with well-defined meniscated backfill, are attributed to *Taenidium* isp., following the criteria outlined by Keighley and Pickering (1994); Fig. 8H). The third morphology is characterized by vertical to inclined burrows that are straight to slightly curved, and possess smooth linings without intersections. They are also visible as circular opening in the bedding plane, and are assigned to the ichnotaxon *Skolithos* isp. Haldeman, 1840 (Fig. 8F).

#### 4.4. Molecular weathering ratios

The calculation of molecular weathering ratios including hydrolysis, calcification, clay content, salinization, oxidation, and the calcium-magnesium weathering index (CALMAG) for the studied Vertisol profiles proved to be an important tool for interpreting paleosol

development (Fig. 9; Table 3). In the examined paleosol profiles, the Bssk horizons exhibit higher hydrolysis ratio values, ranging from 1.68 to 2.59, while the Bss and BCk horizons show low to moderate hydrolysis ratio values, varying from 1.73 to 1.91. The clay content trends suggest low levels of clay accumulation, with values ranging from 0.04 to 0.09, exhibiting little variation throughout the horizons. Salinization values vary from 0.19 to 0.48, indicating a low salt composition during the formation of these paleosols. Calcification trends show higher peaks in the Bssk horizons (1.19 to 2.12) and similar values in the Bss and BCk horizons, ranging from 1.24 to 1.50. The degree of oxidation is elevated in the Bssk and Bss horizons (0.26 to 0.37), particularly in the first and second profiles, which exhibit redoximorphic features. The profiles exhibit low to moderate values of CALMAG, ranging from 32.1 to 46.2.

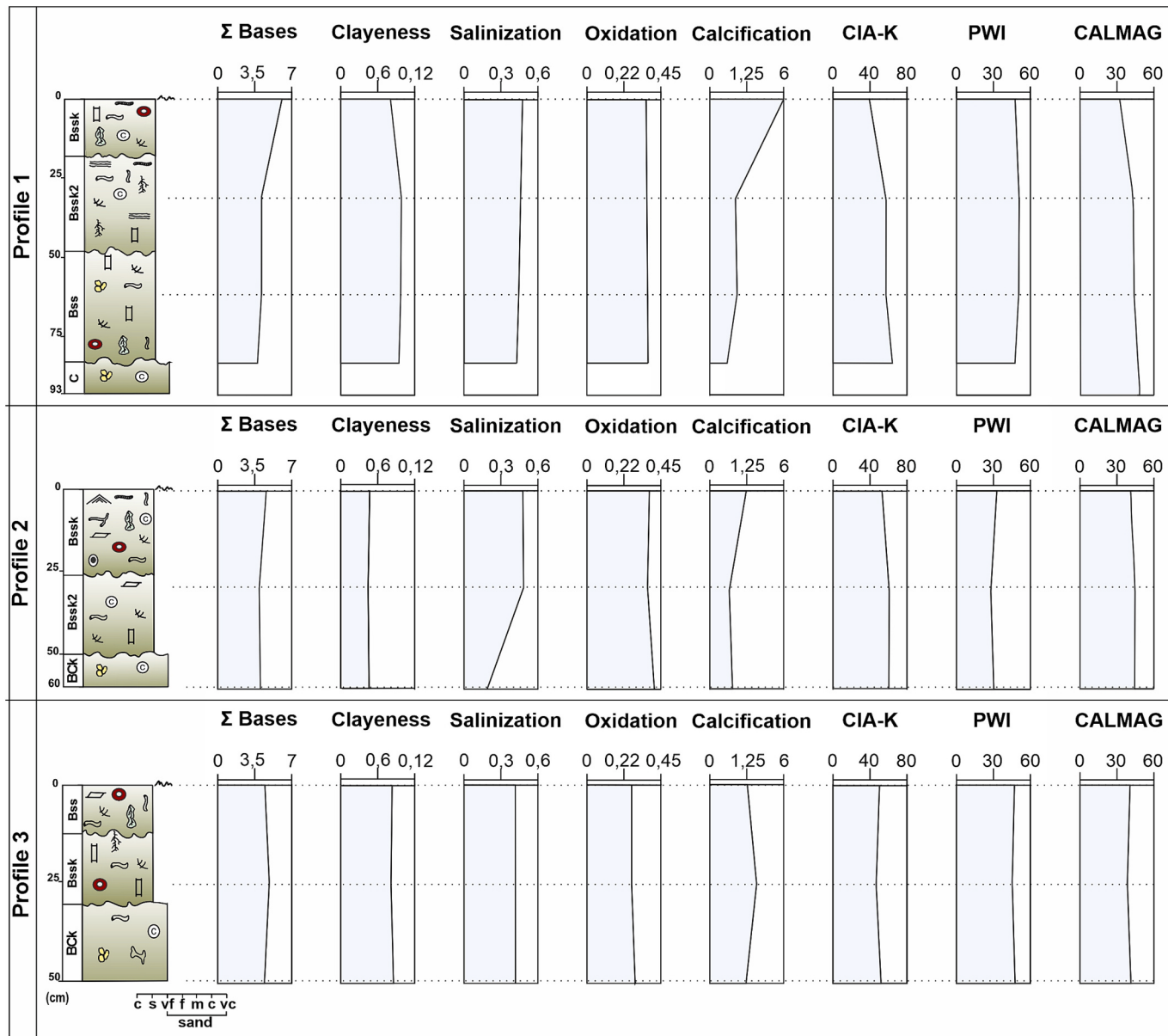


Fig. 9. Distribution of molecular weathering ratios from Serra da Galga Vertisols.

**Table 3**

Results of molecular weathering ratio from Serra da Galga Vertisols and paleoclimate data.

Profile	Horizons	$\Sigma$ Bases	CALMAG	Clay content	Oxidation	Salinization	Calcification	CIA-K	PWI	MAT (PWI)
1	Bssk	2.59	32,1	0.08	0.36	0.48	2.12	39.50	47.73	10.79
	Bssk2	1.77	43,1	0.09	0.37	0.46	1.32	57.58	51.02	10.61
	Bss	1.76	42,9	0.09	0.36	0.44	1.33	57.58	50.59	10.63
	C	–	48,3	–	–	–	–	–	–	–
2	Bssk	1.95	40,3	0.04	0.37	0.48	1.47	53.18	32.62	11.84
	Bssk2	1.68	45,4	0.04	0.37	0.48	1.19	60.82	28.07	12.25
	BCk	1.64	46,2	0.04	0.41	0.19	1.16	63.60	29.61	12.10
3	Bss	1.91	39,9	0.08	0.27	0.42	1.50	50.21	47.10	10.83
	Bssk	2.08	37,5	0.08	0.26	0.42	1.66	46.77	45.40	10.93
	BCk	1.90	40,1	0.08	0.29	0.42	1.48	51.64	47.68	10.80

## 5. Discussion

### 5.1. Maastrichtian paleoclimate reconstruction of the Southern Hemisphere

#### 5.1.1. Reconstruction of regional paleoclimate

The Maastrichtian paleoclimate was characterized by a general global cooling trend, punctuated by two notable warming events (Gómez-Alday et al., 2004; Gao et al., 2015). During this interval, global precipitation levels rose, and average temperatures are estimated to have ranged from 21 °C to 24 °C (Prochnow et al., 2006; Hay and Floegel, 2012). For the Vertisols of the Serra da Galga Member, paleoprecipitation estimates were derived using two geochemical climofunctions. The CALMAG index indicates values ranging from 290 to 614 mm/yr, with a mean of 504 mm/yr and a standard error of  $\pm 33$  mm/yr. In contrast, the CIA-K index suggests higher values, ranging from 481 to 774 mm/yr, with a standard error of  $\pm 30$  mm/yr. A direct comparison reveals a mean paired difference of 150 mm/yr for the CIA-K index, approximately 30 % higher than CALMAG. This discrepancy stems from the fact that CIA-K does not consider MgO and Na<sub>2</sub>O, leading to inflated precipitation estimates whenever CaO is leached, even when substantial Mg remains. The exponential term in CIA-K calculations further amplifies this effect, producing systematically higher MAP estimates. In contrast, CALMAG treats MgO as the swing oxide in Vertisols, retaining it in the denominator. As long as Mg persists, the CALMAG value rises, driving MAP estimates downward. In contrast, CIA-K ignores MgO, causing its denominator to shrink only with Ca loss, and thus pushing CIA-K estimates higher. A similar comparison was developed by Adams et al. (2011), who investigated the reliability of bulk-geochemical weathering indices, specifically CALMAG and CIA-K, for reconstructing mean annual precipitation (MAP) in Vertisols from the Paleocene-Eocene Thermal Maximum (PETM) section of the Bighorn Basin (Wyoming, USA). Their study demonstrated that CIA-K, which excludes MgO, produces artificially elevated MAP estimates due to Ca loss alone, while CALMAG, by incorporating MgO, provides a more consistent and accurate MAP signal. These findings underscore the importance of using Mg-inclusive, linear climofunctions specifically tailored for Vertisols to avoid overestimating precipitation and to improve paleoclimatic reconstructions.

Paleotemperature estimates for these profiles, based on PWI, range from 10.6 °C to 12.2 °C, with an average of 11.1 °C and a standard error of  $\pm 0.62$  °C (Fig. 10A). However, Gallagher and Sheldon (2013) caution that using PWI to estimate MAT in Vertisols may be unreliable because this order soils typically exhibit limited cation leaching compared to forest soils. As a result, smectite remains stable, leading to artificially low PWI values that may not accurately reflect paleotemperatures (Buol et al., 2011; Gallagher and Sheldon, 2013). Consequently, the PWI method is more applicable to soils with Bt horizons and PWI values below 60, since higher PWI values typically indicate limited chemical weathering and, thus, questionable significance for paleotemperature reconstruction (Gallagher and Sheldon, 2013). However, for the Serra da Galga Member Vertisols, the presence of translocation processes,

moderate base accumulation, and PWI values ranging from 31.1 to 46.2 support the application of the PWI-based paleotemperature estimates. These values, alongside careful pedogenic and geochemical interpretations, suggest that while PWI has limitations in Vertisols, it can still provide useful dataset for these particular profiles when applied cautiously.

To define the climate patterns controlling the formation of each paleosol horizon, three aridity indices were employed, each utilizing the same MAT-MAP pairing but applying different temperature weightings. The Lang index (Allang; Lang, 1920) is calculated by dividing mean annual precipitation (MAP, in mm) by mean annual temperature (MAT, in °C), without the addition of a constant. However, in colder climates where MAT values can be negative (MAT < 0 °C), this index may yield artificially inflated values or become inapplicable due to division by zero or a negative denominator. To resolve this issue, the de Martonne (AI<sub>d</sub>M; de Martonne, 1926) and Köppen (AIKöppen; Köppen, 1923) indices incorporate temperature constants of +10 °C and + 33 °C, respectively, into the denominator. The de Martonne index, for example, adds a constant equivalent to the lowest MAT observed in his European dataset (approximately -10 °C), ensuring a consistently positive denominator. This approach enhances reliability by preventing mathematical artifacts in cold conditions. In contrast, the Köppen index applies a larger constant (+33 °C), which disproportionately inflates the denominator, particularly at mid-latitude MAT values of ~10–15 °C, resulting in lower index values and a bias toward drier climate classifications unless precipitation is very high (Quan et al., 2013).

Application of these indices to the Serra da Galga Member samples reveals notable variability in climatic classification. The Lang index classifies 30 % of the samples as semiarid and 70 % as subhumid/humid. Similarly, the de Martonne index yields 30 % semiarid and 70 % subhumid classifications. In contrast, the Köppen index assigns 90 % of the samples to the semiarid category and only 10 % to the subhumid class. These discrepancies underscore the influence of each index's embedded temperature constant on climate interpretation. Notably, the Köppen index, with its conservative bias driven by the large temperature addition, tends to align more closely with the pedogenic evidence observed in these mid-latitude, southern hemisphere Vertisols. Conversely, the Lang and de Martonne indices may overestimate humidity under moderate temperature conditions, highlighting the importance of choosing an appropriate index based on regional paleoclimatic and pedogenic context.

In conjunction with the climofunction-derived estimates, the presence of vertic features, pedogenic carbonate precipitation, gleyzation, redoximorphic features, and iron nodules in the Vertisols of the Serra da Galga Member suggests that the paleoclimate was neither persistently arid nor uniformly dry. These pedogenic attributes develop under distinct hydromedical conditions, indicating that soil formation occurred under fluctuating moisture regimes. The development of vertic horizons, typically associated with floodplain settings or ephemeral lacustrine environments, further supports the occurrence of periodic water accumulation throughout the year. Such hydrological variability promotes shrink-swell dynamics, leading to the formation of wedge-

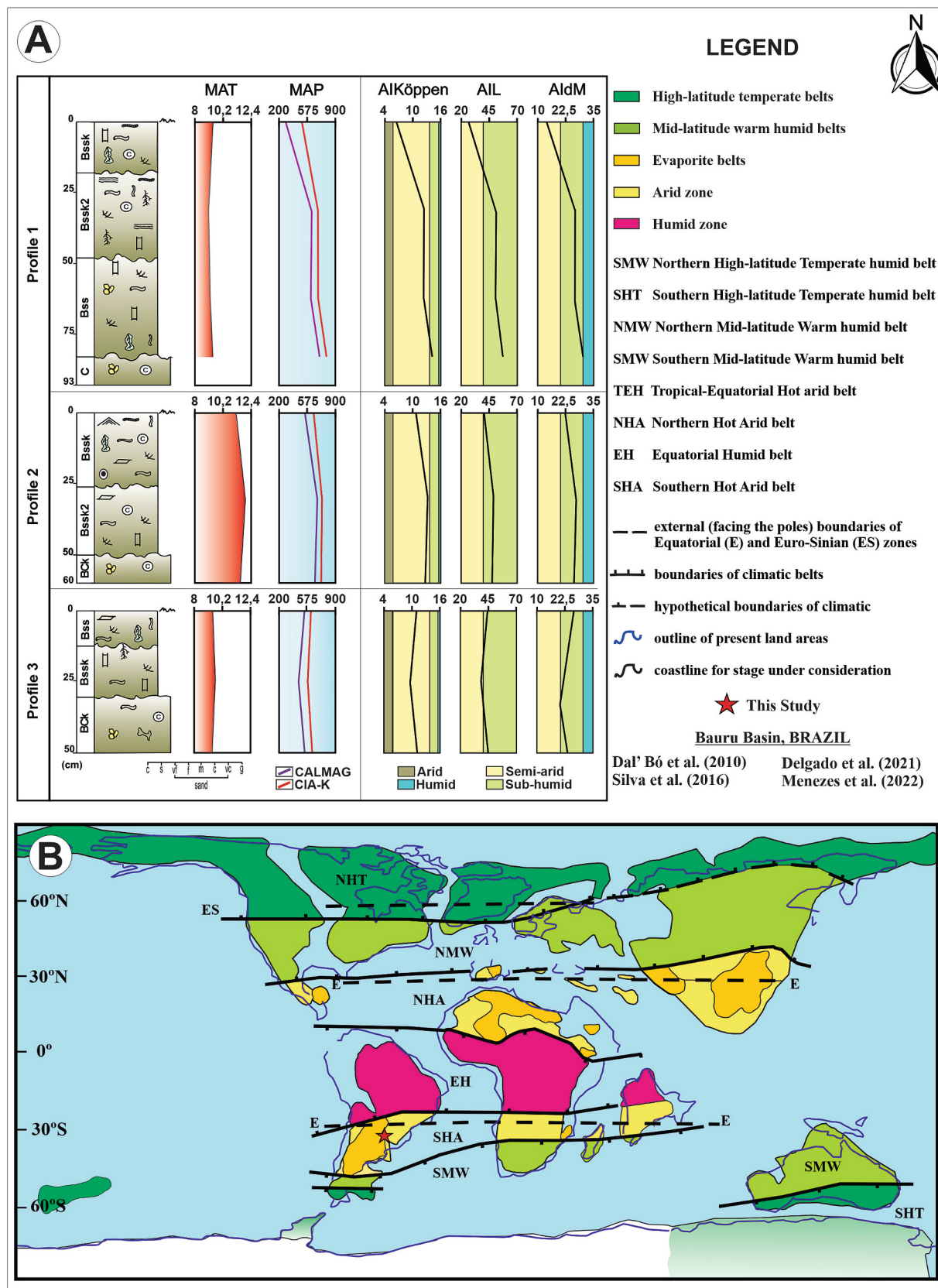


**Fig. 10.** Paleoclimate interpretation during Serra da Galga Member paleosols formation. (A) Köppen aridity index (Köppen AI) estimation curves for the Serra da Galga Vertisols. B) Maastrichtian paleoclimatic reconstruction from Chumakov (2004) modified by Craggs et al. (2012).

shaped pedes and slickensides, which are diagnostic of seasonal cycles of saturation and desiccation (Retallack, 2001).

Micromorphology observations of clay coatings and infillings and the presence of iron oxides were attributed to more humid environmental conditions (Schellmann, 1981; Nettleton et al., 1990; Menezes et al., 2024). The greenish gray color is additional evidence of seasonal wetting conditions, considering that mottling due to seasonal soil saturation is common in modern soils (Retallack, 1990). In contrast, pedogenic calcium carbonate features, such as nodules, typically form under drier conditions with limited moisture availability and are frequently documented in soils from arid to semi-arid environments (Durand et al., 2018). Furthermore, the ichnoassemblage is marked by low density and ichnodiversity, and dominated by ichnotaxa indicative of intermittent colonization, suggesting environmental instability and brief periods of habitability between episodes of flooding and desiccation (Smith et al., 2008; Menezes et al., 2021; Sedorko et al., 2025). This seasonal cycle is further demonstrated by rhizogenic laminar structures and rhizohalos, which forms in response to seasonal humidity fluctuations (Wright et al., 1995).

The clay-mineral assemblage in the Serra da Galga Member Vertisols also reflects the climatic conditions, characterized by smectite (including montmorillonite and nontronite) and sepiolite. The parent material, rich in expandable clays, is associated with continental deposits linked to lacustrine-palustrine environments, as well as soils from arid and semiarid contexts, or early diagenetic transformations (e.g., Velde, 1995; Galán and Pozo, 2011). Pedogenic smectite occurs in intermittently poorly drained environments, typically associated with strongly seasonal precipitation (Khormali and Abtahi, 2003; Meunier, 2005; Sheldon and Tabor, 2009). Sepiolite forms most effectively in environments characterized by moderate precipitation and periodic drying cycles, which promote the concentration of magnesium and silica while maintaining alkaline conditions. However, both extreme aridity and excessive precipitation can disrupt the delicate geochemical balance required for sepiolite precipitation (Birsoy, 2002; Herranz and Pozo, 2022). Such semi-arid to subhumid conditions are also conducive to the development of calcretes, facilitating the accumulation and preservation of calcium in paleosol horizons (Goldberg and Garcia, 2000; Delgado et al., 2021).

### 5.1.2. Southern Hemisphere climate condition

Paleogeographic reconstructions suggest that, during the Maastrichtian, the Marília Formation was situated near the transitional boundary between the Southern Hot Arid Belt (SHA) and the Equatorial Humid Belt (EH; Craggs et al., 2012; Menezes et al., 2022). This paleo-positioning subjected the region to a unique combination of climatic influences, resulting in chemical, pedogenic, and mineralogical characteristics indicative of a semiarid to subhumid environment (Menezes et al., 2022). The studied Vertisols, based on geochemical and micromorphological data, reflect seasonally variable climatic conditions comparable to those described by Menezes et al. (2022), highlighting episodic humid intervals within a predominantly semiarid setting (Fig. 10B). Despite the potential of paleosols as climatic proxies, they remain underutilized in reconstructions of Southern Hemisphere basins. However, select studies from Brazil, Argentina, Madagascar, and India have employed paleosol climofunctions to yield valuable insights into Maastrichtian climate dynamics. In southern Patagonia (ca. 54°S), paleosols from Argentina developed within the mid-latitude warm humid belt, and show evidence of temperate and humid conditions during the Late Cretaceous, contrasting with the semiarid conditions inferred for the Bauru Basin Vertisols (Varela et al., 2017; Raigemborn et al., 2025). Conversely, paleosols from the Deccan Volcanic Province and the Lameta Formation in central India, regions paleolatitudinally equivalent to the Bauru Basin, record temporally and spatially variable aridity and seasonality, pointing to oscillating paleoclimatic regimes (Dzombak et al., 2020; Kumari et al., 2021).

Similarly, Kast et al. (2008) and Ohba et al. (2016), through paleosol

climofunctions and paleoclimate modeling, reported alternating arid to humid conditions in the Maevarano Formation, Mahajanga Basin (Madagascar). Despite all these regions being located within the SHA, the paleosol records consistently indicate episodic humid influences, underscoring the climatic heterogeneity of this belt during the Maastrichtian.

This climatic regime reflects a transition toward a cooler greenhouse state, in contrast to the Early Cretaceous, when Earth was characterized by a hot greenhouse climate marked by high global temperatures, minimal polar ice, elevated atmospheric CO<sub>2</sub> concentrations, and widespread arid regions, particularly in the Southern Hemisphere (Kidder and Worsley, 2012; Hay and Floegel, 2012). By the latest Maastrichtian, the final stage of the Cretaceous, global temperatures had declined to approximately 21 °C to 24 °C, coinciding with limited polar ice formation and increased global precipitation (Prochnow et al., 2006; Flögel et al., 2011; Hay and Floegel, 2012; Kidder and Worsley, 2012). Atmospheric CO<sub>2</sub> concentrations dropped significantly compared to earlier Cretaceous stages, stabilizing between 350 and 750 ppmv. Although transient warming events still occurred, possibly linked to volcanic activity such as the Deccan Traps eruptions, the overall climatic trend was one of gradual global cooling (Ekart et al., 1999; Beerling et al., 2002; Nordt et al., 2002, 2003; Huang et al., 2012; Menezes et al., 2022). Ocean temperatures also decreased, altering heat distribution patterns (Chumakov, 2004; Gómez-Alday et al., 2004; Hunter et al., 2008), which contributed to the contraction of arid zones in the Southern Hemisphere and an increase in rainfall in regions such as Brazil, Africa, and India, alongside the expansion of the Equatorial Humid Belt (EHB).

## 5.2. Vertisol formed in semiarid fluvial floodplain setting

### 5.2.1. Pedogenic processes

The Serra da Galga Member represents the medial zone of a distributive fluvial system, where paleosols formed alongside fluvial sedimentation. Pedogenesis occurred nearly simultaneously with floodplain deposition, and soil development was influenced by sedimentation rates, which declined with distance from the active channels. This gradient led to a spatial distribution of paleosols, from Entisols and weak Inceptisols near channels to well-developed Vertisols in more distal floodplain settings (Dal' Bó et al., 2019; Sedorko et al., 2020). In this study, the Vertisols were characterized through an integrated analysis of their macromorphological and micromorphological features, clay mineral composition, molecular weathering indices, and bioturbation structures. The combined evidence indicates that the primary pedogenic processes involved in their development include argilliturbation, clay illuviation, limited gleyzation, carbonate accumulation, and biological activity.

Pedogenic minerals identified in the paleosols, including smectite, sepiolite, and mica, formed in situ through mineral alteration and eluviation processes. Smectite neoformation is primarily governed by pore-water flux, the availability of base cations (Mg<sup>2+</sup>, Ca<sup>2+</sup>), silica, and alkaline pH conditions (Wilson, 1999; Gürel, 2017). Soil moisture plays a critical role by creating leaching microenvironments that release potassium from mica and enhance the mobility of ions essential for smectite crystallization (Khormali and Abtahi, 2003; Taheri et al., 2019). These conditions typically occur in poorly drained settings with low hydraulic conductivity (Allen and Hajek, 1989). The association of the honeycomb structure of smectite with small pores or as coatings on feldspar minerals indicates in-situ formation. In contrast, the flake-like morphology of smectite that coats grains and fills microfractures suggests downward clay translocation within the profile. According to Iacoviello et al. (2012) and Trzciński and Wójcik (2019), this honeycomb structure forms during wet seasons, when smectite gels infill microcracks; during subsequent drying, the gel partially desiccates but remains adhered to grain and crack walls, preserving a reticulate "skin" with a distinctive honeycomb texture. These fragile, wafer-thin walls

support an in-situ origin, unlike detrital smectite with flake-like habits, which originates from the weathering of soils or volcanic glass, is transported, and subsequently deposited as discrete plate-like particles (Wilson and Pittman, 1977; Ehrmann et al., 2005; Iacoviello et al., 2012). Sepiolite, by contrast, precipitates under moderately alkaline conditions (pH 8.5–9.5), in environments rich in Mg<sup>2+</sup> and silica but low in aluminum. High aluminum concentrations promote the formation of Al-rich clays, such as smectite, while excess calcium fosters carbonate precipitation, which can compete with Mg-silicates and inhibit sepiolite formation (Birsoy, 2002; Herranz and Pozo, 2022). The vertic horizons display high smectite contents (52 %–72 %), accompanied by slickensides, microrelief variation, and surface cracking. Montmorillonite, the dominant smectite mineral, typically forms under slightly acidic, poorly drained conditions and is primarily responsible for the shrink–swell behavior observed in Vertisols. This expansive capacity, caused by water absorption between dioctahedral layers, drives the argilloturbation processes characteristic of these soils (Fig. 11A).

During the dry season, soil contraction caused by water loss leads to the formation of surface cracks, which create channels that may subsequently be filled with surrounding soil material or transported sediments (Stiles et al., 2003; Fig. 11B). Upon soil rewetting, clay hydration induces expansion, closing the cracks and generating internal deformation (Fig. 11B). This cyclical process causes wedge-shaped aggregates to shift against each other along sliding planes, forming slickensides. These pedogenic slickensides develop along planes of weakness in response to the shrink–swell mechanism characteristic of Vertisols (Yaalon and Kalmar, 1978; Aslan and Autin, 1998). Stereographic projections of poles to fold surfaces within the Bssk horizon of Profile 2, combined with slickenside striae analysis, demonstrate that the orientation and dip of the slickensides correspond closely with the slopes of the fold flanks previously described (Fig. 11C). This association suggests that the slickensides are deformation planes directly linked to folding processes involved in pseudo-anticline (mukkara) formation. Additionally, along the slickenside surfaces, the alignment of plasma and mineral grains can be observed. Gray and Nickelsen (1989) attributed slickenside formation to shearing along oblique failure planes, resulting from an imbalance between lateral and vertical stresses within the soil, a mechanism also responsible for mukkara structures (Fig. 11C).

Notably, the quasi-2D expression of mukkara structures illustrated in Fig. 4 likely reflects the influence of the gentle local slope, measured at approximately ~5° toward 222° (SW) over a 5-m transect, corresponding to a 0.42-m elevation difference. Although relatively subtle, this gradient is sufficient to bias passive pedogenic processes, promoting downslope clay movement and preferential slickenside orientation, thereby elongating microrelief features toward the SW. According to Soares et al. (2021), palaeoenvironmental reconstructions of the studied fluvial distributive deposits indicate paleocurrents directed toward the NW. The Vertisols formed within flood basins situated orthogonally (SW) to the channel–levee systems, which display variable elevation gradients from the levee crest toward the flood basin center. This geomorphic context supports the interpretation of a gravitational component influencing mukkara development at the Profile 2 site. Moreover, the presence of rhizogenic features at the top of the Bssk horizon suggests that erosional processes affected the overlying, thin A horizons, removing them without significant incision into deeper soil levels.

The presence of clay microfeatures, such as pore striated b-fabric, parallel striated b-fabric, and capping clay coatings, indicates active clay translocation within the vertic horizons. This process is common in soils with sandy loam textures developed under subhumid to humid conditions, where clay illuviation forms striated b-fabric. Similar micromorphological patterns have been reported in vertic horizons from the United States, Brazil, Argentina, and Iran (Etedali et al., 2018; Ladeira et al., 2022; Lizzoli et al., 2024; Hembree, 2024). Clay translocation is primarily driven by shrink–swell dynamics, biological activity, and water fluxes. Periodic water movement through soil cracks and shear

planes promotes both lateral and vertical redistribution of clay particles and soluble ions (Driese, 2004).

In the studied Vertisols, processes such as calcification, gleyzation, and biological activity are closely linked (Fig. 11D). Under subhumid climates, increased soil moisture creates favorable conditions for plant growth and fixation. The interaction between soil and biota can form and destroy peds, increase soil respiration and acidification process, nutrient cycle and improve the hydraulic conductivity (Hole, 1981; Cunningham et al., 2009; Smith et al., 2011). According to Gocke and Kuzyakov (2011) and Menezes et al. (2021), the expansion of plant roots enhances subsurface respiration and increases the presence of organic acids, which, along with pluvial water, act as primary agents in mineral degradation. When a semiarid climate prevails, plants experience hydric stress due to a pluvial deficit. The stress creates a supersaturated microenvironment around the rhizosphere, where carbonate precipitation occurs, often following root decay (Gocke and Kuzyakov, 2011; Wang et al., 2015; Menezes et al., 2021). This process results in the calcification of the vadose zone, forming localized calcification regions in the soil horizon. The presence of plants and invertebrate burrows represents the modification of groundmass by soil biota (Retallack, 2001; Stoops et al., 2010). In this sense, bioturbation plays a fundamental role in paleosol development, as evidenced by the observed correlation between trace fossil density and pedogenic carbonate accumulation in the studied Vertisols. Horizons exhibiting moderate to high bioturbation levels are consistently associated with increased calcium carbonate concentrations, resulting in the formation of Bssk horizons. Calcite spherulites form similarly to those described by Rodrigues et al. (2019), being associated with the decay of fine horizontal roots and organic matter within invertebrate burrows. This decomposition process raises the alkalinity in micro-zones, creating favorable conditions for carbonate supersaturation. Resident bacteria accelerate this process by altering pH and redox conditions. Consequently, fibro-radial calcite nucleates on organic templates in situ, forming spherulites that typically line rhizohalos and fill the interiors of bioturbation structures. This set of interactions has been documented in the Bauru Basin, particularly within the Marília Formation, where the precipitation and spatial distribution of calcium carbonate have been attributed to both biotic and abiotic processes (Dal'Bó et al., 2010; Silva et al., 2019; Nascimento et al., 2019; Rodrigues et al., 2019; Menezes et al., 2021).

Depletion zones within vertic horizons are typically localized around macropores formed by invertebrate activity and root penetration. In contrast, redox concentrations commonly develop adjacent to these macropores, where iron masses and nodules precipitate. According to Kraus and Hasiotis (2006), Vepraskas (2015), and Menezes et al. (2024), this process is initiated following plant death, when microbial decomposition of organic matter within water-saturated macropores promotes the reduction of Fe and Mn, resulting in bleached or iron-depleted zones. The soluble Fe<sup>2+</sup> is subsequently mobilized and reoxidized to Fe<sup>3+</sup> in oxygenated areas near the macropores, leading to the formation of localized gley features such as pore linings and concentric halos. The differences in pedogenic development among the Vertisol profiles reflect a complex interplay of climatic seasonality, sedimentation rates, drainage conditions, and landscape stability during the Maastrichtian.

#### 5.2.2. Paleoenvironmental interpretation of Vertisol profiles

The Vertisols of the Serra da Galga Formation share key pedogenic, climatic, and environmental traits with vertic soils documented in both modern and ancient contexts worldwide, underscoring their relevance for broader paleoenvironmental comparisons. Modern analogues include floodplain Vertisols from the Lake Chad Basin (Chad, Nigeria, Cameroon; Holocene–present; Pierre et al., 2019), the Deccan Plateau in India (Ahmad, 1996; Pal et al., 2009), the Gezira clay plains of Sudan (El Abedine et al., 1969; Ahmad, 1996), Australia's Darling Downs (Ahmad, 1996; Isbell, 2021), Texas, USA (Wilding et al., 1989; Kishné et al., 2009), and Jordan's limestone plateaus (Sa'eb and Taimeh, 1998). Ancient examples include Devonian Vertisols from North America

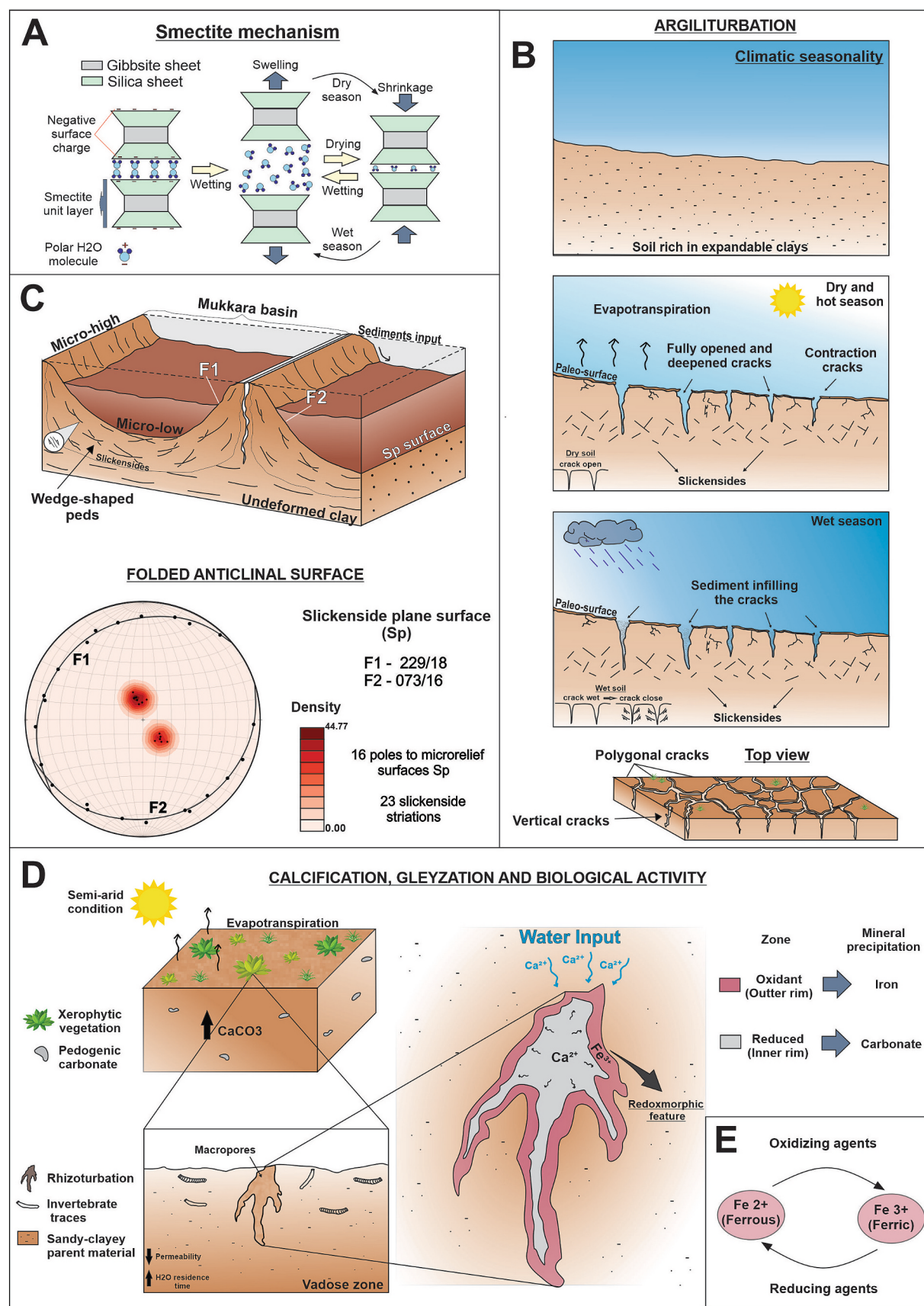


**Fig. 11.** Pedogenic Processes Acting in the Vertisols of the Serra da Galga Member. (A) Smectite shrink-swell behavior. (B) Argilliturbation leading to vertic horizon deformation. (C) Mukkara structure and stereographic projection of data from soil micro-relief structures in the Profile 2. Density contours of pole data to slickensided surfaces (Sp) along with slickenside striations are shown in the plot. (D) Calcification and gleyzation processes, influenced by biogenic activity. (E) Iron mobility in the presence of water.

(Driese and Mora, 1993) and Early Cretaceous (Barremian–Aptian) paleosols from the Yellow Cat Member of the Cedar Mountain Formation in Utah (Joeckel et al., 2017). In all these cases, Vertisols typically develop in low-relief alluvial plains or topographic depressions where fine-grained sediments accumulate under conditions of alternating hydromorphism and seasonal desiccation. These environmental oscillations, combined with smectite-rich clay mineralogy, promote diagnostic morphological features such as slickensides, wedge-shaped aggregates, deep shrink-swell cracks, and, in semi-arid settings, calcic horizon formation.

The Serra da Galga Vertisols conform to this global pattern, having developed in medial-to-distal floodplain settings of a distributive fluvial system, where fluctuating groundwater levels and episodic overbank sedimentation created the hydrological and textural framework necessary for vertic properties to form. The Profile 1 exhibits high levels of mineral alteration, mean annual precipitation (MAP), CALMAG index, clay concentration, and a well-developed striated b-fabric. These features suggest that the clay content derives from both in situ formation and translocation. However, the relatively low smectite content and limited development of slickensides indicate a less advanced stage of internal soil deformation. The moderate to locally high bioturbation index (2–4) reflects significant trace fossils distribution, suggesting that biological activity contributed to clay redistribution. Moderate drainage conditions, marked by episodic water infiltration, are evidenced by redoximorphic features and enhanced macroporosity associated with bioturbation. The presence of a well-formed Bssk horizon, localized carbonate accumulations, abundant biogenic structures, and elevated clay content, despite limited deformation, indicates moderate pedogenic development. These characteristics are consistent with formation under conditions of episodic landscape stability within a dynamic, distal floodplain environment.

In contrast, Profile 2 exhibits lower clay and base content but higher concentrations of sand grains, mineral alteration, MAP, CALMAG index, and striated b-fabric. These characteristics suggest that clay formation resulted from both in situ pedogenesis and translocation. The horizon is distinguished by elevated smectite content, pervasive slickensides, and pseudo-anticlinal structures, all indicative of advanced internal soil deformation. The low clay content likely reflects intensified leaching, driven by the textural features that increases interparticle porosity and promotes vertical and lateral water movement, further enhanced by shrink-swell dynamics. Profile 2 shows moderately well-drained conditions, evidenced by the scarcity of redoximorphic features and the presence of strongly deformed vertic horizons. The pronounced expression of eluviation and episodic infiltration suggests active clay translocation under semi-permeable conditions. Pedogenic development is expressed by localized carbonate accumulation (less abundant than in Profile 1), widespread slickensides, and a high frequency of striated b-fabric. Collectively, these features indicate a moderate to advanced stage of soil development, likely associated with prolonged landscape stability, reduced sedimentation rates, and sustained pedogenic activity. Additionally, lower Profile Weathering Index (PWI) values support the interpretation of a more mature soil, depleted in alkaline elements through prolonged leaching.

Profile 3 is characterized by moderate levels of clay accumulation, MAP, CALMAG index, and the presence of striated b-fabric, suggesting that clay translocation is the dominant process. In contrast, lower mineral alteration levels point to limited in situ clay neoformation. This profile also shows the lowest smectite content among the studied profiles and minimal evidence of internal soil deformation. In the other hand, Profile 3 exhibits somewhat poorly drained conditions, as suggested by the limited internal deformation, localized carbonate accumulation, sparse redoximorphic features, and reduced trace fossil density. The degree of pedogenic development and relative soil maturity are reflected in the presence of carbonate nodules, less abundant than in Profile 1, coupled with low levels of argiloturbation and weakly developed, irregular striated b-fabric. These features indicate an early to

moderate stage of pedogenesis, likely corresponding to a more dynamic depositional setting, such as proximal floodplain areas or near channel margins, where soil formation was periodically interrupted by sediment influx. This interpretation is further supported by the low CALMAG values and high Profile Weathering Index (PWI) values, which collectively indicate limited chemical weathering and relatively immature soil development when compared to a geochemical baseline, such as that represented by the C horizon.

The Vertisols of the Serra da Galga Formation record pedogenic processes, hydrological regimes, and climatic signals consistent with modern and ancient vertic soils formed under seasonal semi-arid to sub-humid conditions. Profile 1, with high clay content, pronounced slickensides, and localized carbonate nodules, aligns with modern Vertisols from the Sudan's Gezira clay plains (El Abedine et al., 1969; Ahmad, 1996), Jordan's limestone plateaus (Sa'eb and Taimeh, 1998), Australia's Darling Downs (Isbell, 2021), and Devonian North America (Driese and Mora, 1993), where alternating flooding and desiccation foster calcic horizons and strong vertic microfabrics. Profile 2, characterized by abundant smectite, pervasive argiloturbation, and reduced carbonate, parallels Vertisols of India's Deccan Plateau (Pal et al., 2009) and distal floodplains of the Yellow Cat Member, Utah (Joeckel et al., 2017), where low sediment input and better drainage sustain prolonged pedogenesis. In contrast, Profile 3 resembles Vertisols from the Lake Chad Basin margins (Pierre et al., 2019), both showing less mature vertic development and stronger hydromorphic influence, resulting in reduced vertic features, lower smectite content, and patchy carbonate accumulations. These similarities arise from formation in medial-to-distal floodplain settings, where seasonal waterlogging alternated with intense drying, producing smectitic shrink-swell clays, wedge-shaped peds, deep cracks, and, in drier cases, calcic horizons. Collectively, these profiles demonstrate strong affinities with Vertisols from global wet-dry semi-arid floodplain systems, reinforcing their value for paleoenvironmental reconstruction.

### 5.3. Paleoecology

The ichnofossil assemblage preserved in the Serra da Galga Vertisols consists of traces from invertebrates (*Skolithos*, *Taenidium* and *Beaconites*) and plants (calcareous rhizoconcretions, rhizohalos, and calcified plant bulbous structures). This assemblage exhibits low to moderate ichnodiversity and reflects colonization of a floodplain within a medial distributive fluvial system (Fig. 12A). The bioturbation degree ranges from 1 to 3, only locally reaching 4. The presence of rhizoliths and invertebrate trace fossils indicate significant bioturbation of the groundmass by soil biota (Retallack, 2001; Stoops et al., 2010). Vertisols at a lower to moderate stage of development typically form over relatively short timescales, often within a few hundred years (Ahmad, 1983), indicating episodes of landscape stability conducive to soil formation (Kraus, 1999). These conditions allowed for the rapid colonization of the soil by plants and invertebrates, reflecting periods of subaerial exposure and active pedogenesis (Retallack, 1990; Wright, 1992).

The absence of horizon A, marked by an erosional surface and the presence of branched and lateralized shallow roots with depths ranging from 10 to 25 cm, often truncated at the top, suggests a shallow vadose zone. This indicates that the top of the eroded profile was relatively close, as colonization extended only to horizon B. In modern Vertisols, the A horizon is often only a few centimeters thick or entirely absent on microknolls within the Mukkara structure (Soil Survey Staff, 2022). Although vegetation is not considered a major factor in the formation and development of Vertisols, it influences evapotranspiration, the soil water regime, and soil properties (Coulombe et al., 1996a, 1996b). Vertisols are typically associated with grass-dominated vegetation in grassland and savanna ecosystems, particularly in regions such as Ethiopia (Africa), northeastern Australia, central India, and eastern Texas (USA; Soil Survey Staff, 2022; Hovenden et al., 2008; Dusal, 1965;

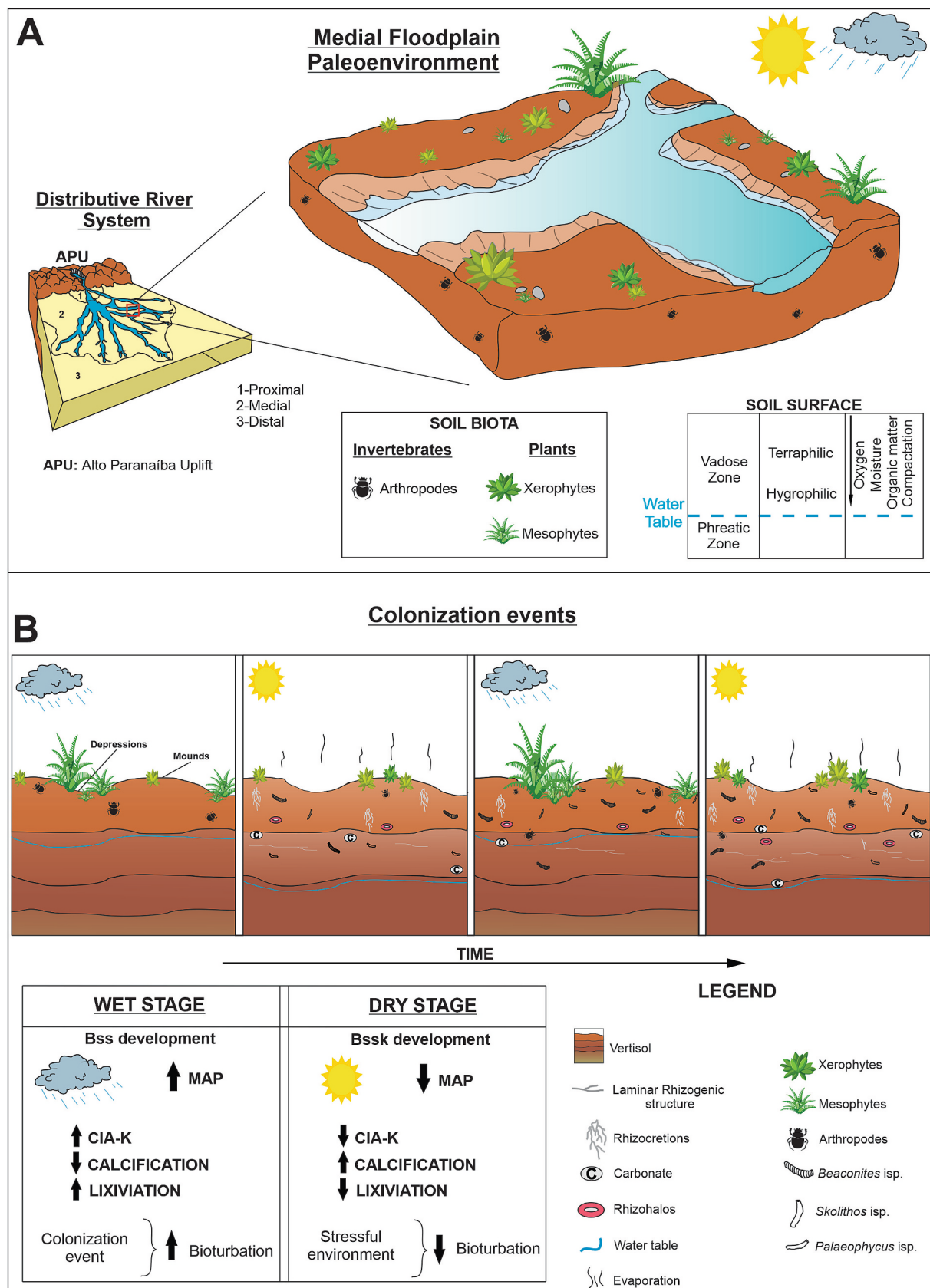


**Fig. 12.** Paleoecological Scenario of the Serra da Galga Member. (A) Paleoenvironmental and paleoecological reconstruction of Serra da Galga Member Vertisols. (B) Colonization events of invertebrate organisms and plants in relation to water table fluctuations, influenced by climatic cyclicity.

Probert et al., 1987; Coulombe et al., 1996a, 1996b). Differences in vegetation are good indicators of surface variability in Vertisols with microrelief. Generally, xerophytic plants dominate mounds, while mesophytic vegetation occupies depressions (e.g., Coulombe et al., 1996a, 1996b; Fig. 12B). Both plant types were present during the Cretaceous period, as evidenced by macrofloras and palynofloras (Frederiksen, 1972; Rodríguez-Barreiro et al., 2022; Friis et al., 2021; Herman and Domogatskaya, 2023; Espronceda et al., 2024; Cambria et al., 2025).

Based on the root system classification proposed by Cannon (1949), which analyzes root morphology and branching order, the studied root traces can be interpreted as 'type four'. Type four roots are associated with xerophytic or mesophytic plants, characterized by a long, slender primary root and well-branched first-order lateral roots. In paleosols, these horizontal, branched roots often form rhizogenic laminar structures during diagenesis following root decay. Such structures are commonly found in aggrading floodplain systems, where shallow water tables and seasonal moisture variations create conditions favorable for carbonate precipitation (Wright et al., 1995), and similar to the structure described in studied Vertisols. Bulbous structures identified in the studied Vertisols, featuring concentric spherical bodies with rings radiating from the center, can be interpreted as rhizosphere calcification, consistent with the descriptions of Singh and Srivastava (2021). According to these authors, such bulb-like morphologies form primarily through biogenic and geochemical processes in soil niches associated with plant roots. Root secrete exudates create localized microenvironments that promote microbial colonization, thereby accelerating calcium carbonate ( $\text{CaCO}_3$ ) precipitation within the niches formed by root-microbe interactions. The centrifugal movement of calcium-rich solutions often results in the development of concentric or nodular structures around the root systems. Additionally, the decomposition of organic matter alters soil pH, further promoting  $\text{CaCO}_3$  precipitation. Alternating wet and dry cycles enhance the mobility and subsequent precipitation of minerals within soil pores, contributing to the formation of these bulbous structures. This seasonal cycle is also evidenced by the formation of rhizohalos, which develop under specific conditions of saturation with stagnant water following root decay, and by calcareous rhizoconcretions, which form under enhanced evaporative conditions.

The invertebrate ichnofossils preserved in the paleosols provide valuable insights into ethological interpretations. The occurrence of *Beaconites* and *Taenidium* in high local densities suggests a complex ethological pattern, likely involving multiple phases of burrow occupation by distinct tracemakers or successive generations of similar organisms in a changing substrate. The variability in burrow diameters supports different populations, potentially reflecting ontogenetic stages or functional differentiation among the burrowers. Such trace fossil assemblages are interpreted as opportunistic colonization events, responding to fluctuations in sediment moisture or water table levels, and indicating episodic availability of favorable conditions for infaunal activity (Graham and Pollard, 1982). The formation of *Beaconites* and *Taenidium* has been primarily attributed to worms (Laming, 1970; Gevers et al., 1971) or arthropods (Müller, 1975; Rolfe, 1980; Allen and Williams, 1981), while for the Marília Formation *Taenidium* has been also attributed to beetles' larvae (Nascimento et al., 2022).

The burrows described here do not present clear faecal back-packing, what would allow the attribution to worms, as proposed by Gevers et al. (1971), while the locomotors back-packing behavior of arthropods (Müller, 1975) is more plausible. The meniscus structures support this interpretation, as they feature frequent lateral offsets, indicating limited lateral flexibility of a short-bodied burrower rather than the smooth, rectilinear movement typical of worm-like organisms (e.g., Graham and Pollard, 1982). Typically, the depth of burrows produced by beetles' larvae corresponds to the minimum depth of the unsaturated zone (Hasiotis, 2002). Finally, *Skolithos* is commonly interpreted as a dwelling burrow in continental environments, probably produced by arthropods (e.g., Sedorko et al., 2024). Its occurrence in paleosols is typically

associated with the activity of excavating arthropods, such as arachnids, coleopterans (beetles), and bees, as well as annelids (Ratcliffe and Fagerstrom, 1980; Schlirf et al., 2001; Buatois and Mángano, 2004; Netto, 2007; Gregory et al., 2009). The distribution of *Skolithos* is influenced by multiple environmental factors. The primary controls include soil type and water availability (Serrano, 1994), while secondary influences include vegetation cover, flood frequency, nutrient availability, and climatic seasonality (Pearson and Gingras, 2006; Nascimento and Netto, 2019).

The here described trace fossil association indicates the presence of organisms inhabiting the upper part of the vadose zone and the upper soil-water profile (terraphilic), according to Hasiotis (2002) classification (Fig. 12A). These traces are indicative of low humidity, where variations in the bioturbation degree reflect cycles of soil moisture driven by periodic precipitation (Hasiotis, 2002; Smith et al., 2008; Fig. 12B). In the Serra da Galga Member Vertisols, periods of water retention within the horizons are primarily influenced by the parent material and climatic seasonality. The combination of sandy and muddy textures, base cation depletion zones, and macropores created by biological activity suggests moderate drainage conditions. These conditions are characterized by shorter flood periods in the floodplain, followed by longer dry seasons.

## 6. Conclusions

The Vertisols of the Serra da Galga Member (Marília Formation, Bauru Basin) developed on floodplain deposits within a distributive fluvial system under a distinctly seasonal climatic regime. Paleoclimatic estimates derived from the CALMAG climofunction indicate mean annual precipitation (MAP) values ranging from 290 to 614 mm/yr, with an average of 504 mm/year and a standard error of  $\pm 33$  mm/year. Mean annual temperature (MAT) estimates, calculated using the Profile Weathering Index (PWI), range from 10.6 °C to 12.2 °C, with a mean of 11.1 °C and a standard error of  $\pm 0.62$  °C. According to the Köppen aridity index, these values suggest a semiarid to subhumid paleoclimate during the period of pedogenesis. During the Maastrichtian, the Marília Formation was situated near the transitional zone between the Southern Hot Arid Belt (SHA) and the Equatorial Humid Belt (EHB), a position that facilitated periodic increases in humidity within an overarching semiarid context. These fluctuating climatic conditions exerted a direct influence on the geochemical, mineralogical, and pedogenetic characteristics of the unit.

The identified pedogenic processes include pronounced argilliturbation, clay illuviation, pedogenic carbonate precipitation, localized gleyization, and intense bioturbation. The abundance of smectitic clays promoted internal deformation and the development of characteristic vertic features such as slickensides and wedge-shaped peds. Calcification and gleyization were closely associated with biological activity, particularly the formation of macropores by roots and invertebrates. These macropores enhanced permeability, facilitated water and solute fluxes, and favored the precipitation of pedogenic carbonates. Redoximorphic features, often surrounding rhizogenic structures, point to iron mobilization and reprecipitation under fluctuating redox conditions. The paleobiota, interpreted from the ichnofossil record and associated morphologies, reveals the coexistence of xerophytic and mesophytic vegetation, an interpretation consistent with known Maastrichtian macroflora and palynoflora. The vertical stratification of biogenic structures and the variation in ichnodiversity across profiles suggest episodic shifts between low and moderate moisture conditions. Soil water retention was modulated by differences in paleosol texture and seasonal precipitation regimes. Collectively, these findings emphasize the strong influence of climate on biotic colonization and pedogenesis, which together governed the formation and evolution of the Serra da Galga Vertisols.

## CRediT authorship contribution statement

**Vithor Di Donato:** Writing – review & editing, Writing – original draft, Conceptualization. **Maurícius Nascimento Menezes:** Writing – review & editing, Writing – original draft, Visualization, Validation, Supervision, Conceptualization. **Patrick Führ Dal' Bó:** Writing – review & editing, Supervision. **Daniel Sedorko:** Writing – review & editing, Supervision. **Jon J. Smith:** Writing – review & editing, Supervision. **Leonardo Borghi:** Writing – review & editing, Supervision.

## Declaration of competing interest

The authors declare no conflict of interest with any research or institution.

## Acknowledgments

The data for this study were provided through the R&D project ANP 20225-9, titled “PRESALT - Geological Characterization of Carbonate Reservoirs from the Pre-Salt Interval of the Santos Basin, Correlates (Sergipe-Alagoas Basin), and Analogues” (UFRJ/Shell Brasil/ANP), sponsored by Shell Brasil. Special thanks to Amanda Goulart Rodrigues for her essential contribution to data acquisition, which was fundamental to this research. The authors also extend their gratitude to the Laboratory of Sedimentary Geology (Lagesed) at the Federal University of Rio de Janeiro for providing the necessary infrastructure for this study. DS thanks the National Council for Scientific and Technological Development (CNPq) for the research grant (CNPq 306493/2022-5 process), and Alexander von Humboldt-Stiftung for post-doc fellowship.

## Data availability

No data was used for the research described in the article.

## References

- Adams, J.S., Kraus, M.J., Wing, S.L., 2011. Evaluating the use of weathering indices for determining mean annual precipitation in the ancient stratigraphic record. *Palaeogeogr. Palaeoclimatol. Palaeoecol.* 309 (3–4), 358–366.
- Ahmad, N., 1983. Vertisols. In: *Developments in soil Science*, 11. Elsevier, pp. 91–123.
- Ahmad, N., 1996. Occurrence and distribution of Vertisols. In: *Developments in Soil Science*, vol. 24. Elsevier, pp. 1–41.
- Allen, B.L., Hajek, B.F., 1989. Mineral occurrence in soil environments. *Miner. Soil Environ.* 1, 199–278.
- Allen, J.R.L., Williams, B.P.J., 1981. Sedimentology and stratigraphy of the Towns- end Tuff Bed (lower Old Red Sandstone) in South Wales and the Welsh Borders. *J. Geol. Soc. Lond.* 138, 15–29.
- Aslan, A., Autin, W.J., 1998. Holocene flood-plain soil formation in the southern lower Mississippi Valley: implications for interpreting alluvial paleosols. *Geol. Soc. Am. Bull.* 110, 433–449.
- Bardgett, R., 2005. *The Biology of Soil: A Community and Ecosystem Approach*. Oxford university press.
- Basilici, G., Dal'Bó, P.F., Oliveira, E.F., 2016. Distribution of palaeosols and deposits in the temporal evolution of a semiarid fluvial distributary system (Bauru Group, Upper cretaceous, SE Brazil). *Sediment. Geol.* 341, 245–264.
- Batezelli, A., 2003. Análise da sedimentação cretácea no Triângulo Mineiro e sua correlação com áreas adjacentes. Tese de Doutorado. Universidade Estadual Paulista (Unesp) Rio Claro, p. 195.
- Batezelli, A., 2015. Continental systems tracts of the Brazilian cretaceous Bauru Basin and their relationship with the tectonic and climatic evolution of South America. *Basin Res.* 29, 1–25.
- Batezelli, A., Ladeira, F.S.B., Nascimento, D.L., Silva, M.L., 2019. Facies and palaeosol analysis in a progradational distributive fluvial system from the Campanian-Maastrichtian Bauru Group, Brazil. *Sedimentology* 66, 699–735.
- Beerling, D.J., Lomax, B.H., Royer, D.L., Upchurch Jr., G.R., Kump, L.R., 2002. An atmospheric p CO<sub>2</sub> reconstruction across the Cretaceous-Tertiary boundary from leaf megafossils. *Proceedings of the National Academy of Sciences* 99 (12), 7836–7840.
- Birkeland, P., 1999. *Soils and Geomorphology*. Oxford University Press, New York, p. 448.
- Birsoy, R., 2002. Formation of sepiolite-palygorskite and related minerals from solution. *Clay Clay Miner.* 50, 736–745.
- Bromley, R.G., 1996. *Trace Fossils: Biology, Taphonomy and Applications*. Chapman & Hall London, p. 361.
- Buatois, L.A., Mángano, M.G., 2002. Trace fossils from Carboniferous floodplain deposits in western Argentina: implications for ichnofacies models of continental environments. *Palaeogeogr. Palaeoclimatol. Palaeoecol.* 183, 71–86.
- Buatois, L.A., Mángano, M.G., 2004. Animal-substrate interactions in freshwater environments: applications of ichnology in facies and sequence stratigraphic analysis of fluvio-lacustrine successions. *Geol. Soc. Lond. Spec. Publ.* 228, 311–333.
- Bullock, P., Fedoroff, N., Jongerius, A., Stoops, G., Tursina, T., 1985. *Handbook for Soil Thin Section Description*. Waine Research Publication, Wolverhampton.
- Buol, S.W., Southard, R.J., Graham, R.C., McDaniel, P.A., 2003. *Soil Genesis and Classification*, vol. 5. Black Well Pub. Com., Ames, p. 494.
- Buol, S.W., Southard, R.J., Graham, R.C., McDaniel, P.A., 2011. *Soil Genesis and Classification*. John Wiley & Sons, New York, p. 560.
- Cambria, V., Nascimento, D.L., Alessandretti, L., Rangel, C.C., Sedorko, D., 2025. Root trace fossils as indicators of biogeomorphological stages in a cretaceous fluvial system: Insights from the Sanfranciscana basin. *J. S. Am. Earth Sci.* 165, 105724.
- Candeiro, C.R.A., Rich, T., 2010. Overview of the late cretaceous Biota of the western São Paulo State, Brazil, Bauru Group. *J. S. Am. Earth Sci.* 29, 346–353.
- Cannon, W.A., 1949. A tentative classification of root systems. *Ecology* 30, 542–548.
- Carvalho, I.S., Gasparini, Z.B., Salgado, L., Vasconcellos, F.M., Marinho, T.S., 2010. Climate's role in the distribution of the cretaceous terrestrial Crocodyliformes throughout Gondwana. *Palaeogeogr. Palaeoclimatol. Palaeoecol.* 297, 252–262.
- Catt, J.A., 1990. *Paleopedology Manual*. Quaternary International six. Pergamon Press, London.
- Caudill, M.R., Driese, S.G., Mora, C.I., 1996. Preservation of a paleo-Vertisol and an estimate of late Mississippian paleoprecipitation. *J. Sediment. Res.* 66 (1), 58–70.
- Chumakov, N.M., 2004. In: Semikhatov, M.A., Chumakov, N.M. (Eds.), *Climatic Zones and Climate of the Cretaceous period. Climate in the Epochs of Major Biospheric Transformations*, 550. Transactions of the Geological Institute of the Russian Academy of Sciences, pp. 105–123.
- Coulombe, C.E., Dixon, J.B., Wilding, L.P., 1996a. Developments in soil Science. Mineralogy and chemistry of Vertisols, 24. Elsevier, pp. 115–200.
- Coulombe, C.E., Wilding, L.P., Dixon, J.B., 1996b. Overview of Vertisols: characteristics and impacts on society. *Adv. Agron.* 57, 289–375.
- Crags, H.J., Valdes, P.J., Widdowson, M., 2012. Climate model predictions for the latest cretaceous: an evaluation using climatically sensitive sediments as proxy indicators. *Palaeogeogr. Palaeoclimatol. Palaeoecol.* 315, 12–23.
- Cunningham, K.J., Sukop, M.C., Huang, H., Alvarez, P.F., Curran, H.A., Renken, R.A., Dixon, J.F., 2009. Prominence of ichnologically influenced macroporosity in the karst Biscayne aquifer: stratiform “super-K” zones. *Geol. Soc. Am. Bull.* 121, 164–180.
- Dal'Bó, P.F.F., Soares, M.V.T., Basilici, G., Rodrigues, A.G., Menezes, M.N., 2019. Spatial variation in distributive fluvial system architecture of the Upper cretaceous Marília Formation, SE Brazil. *Geol. Soc. Lond. Spec. Publ.* 488, 97–118.
- Dal'Bó, P.F.F., Basilici, G., 2010. Estimativas de paleoprecipitação e gênese de feições cárnicas e argilicas em paleosolos da Formação Marília (Neocretáceo da Bacia Bauru). *Geosciences = Geociências* 29, 33–49.
- Dal'Bó, P.F.F., Basilici, G., Angélica, R.S., Ladeira, F.S.B., 2009. Paleoclimatic interpretations from pedogenic calcrites in a Maastrichtian semi-arid eolian sand-sheet paleoenvironment: Marília Formation (Bauru Basin, southeastern Brazil). *Cretac. Res.* 30, 659–675.
- Dal'Bó, P.F.F., Basilici, G., Angélica, R.S., 2010. Factors of paleosol formation in a late cretaceous eolian sand sheet paleoenvironment, Marília Formation, Southeastern Brazil. *Palaeogeogr. Palaeoclimatol. Palaeoecol.* 292, 349–365.
- de Martonne, E., 1926. Aréisme et indice d'aridité. *Comptes Rendus de l'Académie des Sciences* 182, 1395–1398.
- Delgado, L., Batezelli, A., Ladeira, F.S.B., 2021. Paleoenvironmental and paleoclimatic reconstruction of lower to Upper cretaceous sequences of the Bauru Basin based on paleosol geochemistry and mineralogical analyses. *Palaeogeogr. Palaeoclimatol. Palaeoecol.* 569, 110328.
- Dias, A.N.C., Chemale Jr., F., Hackspacher, P.C., Soares, C.J., O-Aristizabal, C.I., Tello, C. A.S., 2018. Fission track and U-Pb double dating of detrital zircon applied to the intracratonic Mesozoic Bauru Basin, Brazil. *Geol. J.* 53, 1767–1780.
- Dias-Brito, D., Musacchio, E.A., De Castro, J.C., Maranhão, M., Suárez, J.M., Rodrigues, R., 2001. Grupo Bauru: uma unidade continental do Cretáceo no Brasil: concepções baseadas em dados micropaleontológicos, isótopos e estratigráficos. *Rev. Paléobiol.* 20, 245–304.
- Dickson, J.A.D., 1965. A Modified Staining Technique for Carbonates in thin section. *Nature* 205, 587.
- Driese, S.G., 2004. Pedogenic translocation of Fe in modern and ancient Vertisols and implications for interpretations of the Hekpoort paleosol (2.25 Ga). *J. Geol.* 112, 543–560.
- Driese, S.G., Mora, C.I., 1993. Physico-chemical environment of pedogenic carbonate formation in Devonian vertic paleosols, Central Appalachians, USA. *Sedimentology* 40 (2), 199–216.
- Driese, S.G., Ober, E.G., 2005. Paleopedologic and paleohydrologic records of precipitation seasonality from early Pennsylvanian “underclay” paleosols, USA. *J. Sediment. Res.* 75 (6), 997–1010.
- Driese, S.G., Mora, C.I., Stiles, C.A., Joeckel, R.M., Nordt, L.C., 2000. Mass-balance reconstruction of a modern Vertisol: implications for interpreting the geochemistry and burial alteration of paleo-Vertisols. *Geoderma* 95, 179–204.
- Dudal, R., 1965. Dark Clay Soils of Tropical and Subtropical Regions, 83. FAO Development Papers, p. 161.
- Durand, N., Monger, H.C., Canti, M.G., 2018. Interpretation of Micromorphological Features of Soils and Regoliths. Calcium carbonate features. Elsevier, Amsterdam, pp. 149–194.

- Dzombak, R.M., Sheldon, N.D., Mohabey, D.M., Samant, B., 2020. Stable climate in India during Deccan volcanism suggests limited influence on K-Pg extinction. *Gondwana Res.* 85, 19–31.
- Ehrmann, W., Setti, M., Marinoni, L., 2005. Clay minerals in Cenozoic sediments off Cape Roberts (McMurdo Sound, Antarctica) reveal palaeoclimatic history. *Palaeogeogr. Palaeoclimatol. Palaeoecol.* 229 (3), 187–211.
- Ekart, D.R., Cerling, T.E., Montanez, I.P., Tabor, N.J., 1999. A 400 million year carbon isotope record of pedogenic carbonate; implications for paleotomospheric carbon dioxide. *Am. J. Sci.* 299 (10), 805–827.
- El Abedine, A.Z., Robinson, G.H., Tyego, J., 1969. A study of certain physical properties of a vertisol in the Gezira area, Republic of Sudan. *Soil Sci.* 108 (5), 359–366.
- Espronceda, P.M., Rodríguez-Barreiro, I., Pérez-Pueyo, M., Bádenas, B., Canudo, I., Puertolas-Pascual, E., Santos, A.A., Diez, J.B., 2024. Palynostratigraphical review of the K-Pg boundary from the Ibero-Armorican Island: New data from the Maastrichtian dinosaur outcrop Veracruz I (Pyrenees, NE Iberian Peninsula). *Cretac. Res.* 154, 10575.
- Etedali, S., Abtahi, S.A., Salehi, M.H., Givi, J., Farpoor, M.H., Baghernejad, M., 2018. Chemical, Physical, Mineralogical and Micromorphological Properties of Soils along a Toposequence in Chelgerd Region, Chaharmahal-va-Bakhtiari, Iran.
- Fernandes, L.A., Coimbra, A.M., 1996. A Bacia Bauru (Cretáceo Superior, Brasil). *An. Acad. Bras. Cienc.* 68, 195–205.
- Flögel, S., Wallmann, K., Kuhnt, W., 2011. Cool episodes in the Cretaceous—Exploring the effects of physical forcings on Antarctic snow accumulation. *Earth Planet. Sci. Lett.* 307 (3–4), 279–288.
- Folk, R.L., 1993. SEM imaging of bacteria and nannobacteria in carbonate sediments and rocks. *J. Sediment. Res.* 63 (5), 990–999.
- Frederiksen, N., 1972. Toward a taxonomy of situations. *Am. Psychol.* 27, 114.
- Friis, E.M., Crane, P.R., Pedersen, K.R., 2021. Microsporangiophores from the early cretaceous (Berriasian) of Bornholm, Denmark, with comments on a pre-angiosperm xerophytic flora. *Rev. Palaeobot. Palynol.* 293, 104487.
- Galán, E., Pozo, M., 2011. Developments in Clay Science Polygorskite and Sepiolite Deposits in Continental Environments. Description, Genetic Patterns and Sedimentary Settings, 3. Elsevier, pp. 125–173.
- Gallagher, T.M., Sheldon, N.D., 2013. A new paleothermometer for forest paleosols and its implications for Cenozoic climate. *Geology* 41, 647–650.
- Gao, Y., Ibarra, D.E., Chengshan, W., Caves, J.K., Chamberlain, C.P., Graham, S.A., Wu, H., 2015. Mid-latitude terrestrial climate of East Asia linked to global climate in the late cretaceous. *Geology* 18, 287–290.
- Gevers, T.W., Frakes, L.A., Edwards, L.N., Marzolf, J.E., 1971. Trace fossils in the lower Beacon sediments (Devonian) Darwin Mountains, southern Victoria Land, Antarctica. *J. Palaeontol.* 45, 81–94.
- Gingras, M.K., MacEachern, J.A., Dashtgard, S.E., 2011. Process ichnology and the elucidation of physico-chemical stress. *Sediment. Geol.* 237, 115–134.
- Gobbo-Rodrigues, S.R., 2001. *Carófitas e ostracodes do Grupo Bauru, Cretáceo Superior continental do sudeste do Brasil*. Doctoral dissertation, Instituto de Geociências e Ciências Exatas da Universidade Estadual Paulista.
- Gocke, M., Kuzyakov, Y., 2011. Effect of temperature and rhizosphere processes on pedogenic carbonate recrystallization: relevance for paleoenvironmental applications. *Geoderma* 166, 57–65.
- Goldberg, K., Garcia, A.J., 2000. Palaeobiogeography of the Bauru Group, a dinosaur-bearing cretaceous unit, northeastern Paraná Basin, Brazil. *Cretac. Res.* 21, 241–254.
- Gómez-Alday, J.J., López, G., Elorza, J., 2004. Evidence of climatic cooling at the early/late Maastrichtian boundary from inoceramid distribution and isotopes: Sopelana sections, Basque Country, Spain. *Cretac. Res.* 25, 649–668.
- Goulart, V.R.C., Verde, M., Manhães, M.T., Mello, C.L., West, D.C., Ramos, K.S., Donato, V., Ferreira, L.C.S., Sedorko, D., 2025. Trace fossil analysis in the Miocene Pindamonhangaba F1 formation, Taubaté Basin. *J. S. Am. Earth Sci.* (in press, 1–11).
- Graham, J.R., Pollard, J.E., 1982. Occurrence of the trace fossil Beaconites antarcticus in the lower Carboniferous fluvio-deltaic rocks of County Mayo, Ireland. *Palaeogeogr. Palaeoclimatol. Palaeoecol.* 38, 257–268.
- Gray, M.B., Nickelsen, R.P., 1989. Pedogenic slickensides, indicators of strain and deformation processes in redbed sequences of the Appalachian foreland. *Geology* 17, 72–75.
- Gregory, M.R., Campbell, K.A., Alfaro, A.C., Hudson, N., 2009. Bee and ant burrows in Quaternary “coffee rock” and Holocene sand dunes, Kowhai Bay, Northland, New Zealand. *Palaeogeogr. Palaeoclimatol. Palaeoecol.* 273, 102–110.
- Gürel, A., 2017. Geology, mineralogy, and geochemistry of late Miocene paleosol and calcrite in the western part of the Central Anatolian Volcanic Province (CAVP), Turkey. *Geoderma* 302, 22–38.
- Haldeman, S.S., 1840. Supplement to number one of ‘A monograph of the Limniidae, and other freshwater bivalve shells of the apparently new animals in different classes, and names and characters of the subgenera in Paludina and Anculosa’. *J. Dobson, Philadelphia* 3.
- Hasiotis, S.T., 2002. Continental Trace Fossils. Society of Economic Paleontologists and Mineralogists, Short Course, Oklahoma, p. 132.
- Hasiotis, S.T., Kraus, M.J., Demko, T.M., 2007. Climatic controls on continental trace fossils. In: Miller III, W. (Ed.), *Trace Fossils: Concepts, Problems, Prospects*. Elsevier, Amsterdam, pp. 172–195.
- Hay, W.W., Floegel, S., 2012. New thought about the cretaceous climate and oceans. *Earth Sci. Rev.* 115, 262–272.
- Hembree, D.I., 2024. Changes in soils and terrestrial landscapes of the Appalachian Basin (Conemaugh, Monongahela, and Dunkard groups), USA, at the onset of the late Paleozoic climate transition. *J. Sediment. Res.* 94 (5), 617–640.
- Hembree, D.I., Blair, M.G., 2016. A paleopedological and ichnological approach to interpreting spatial and temporal variability in early Permian fluvial deposits of the lower Dunkard Group, West Virginia, USA. *Palaeogeogr. Palaeoclimatol. Palaeoecol.* 454, 246–266.
- Hembree, D.I., Nadon, G.C., 2011. A paleopedologic and ichnologic perspective of the terrestrial Pennsylvanian landscape in the distal Appalachian Basin, USA. *Palaeogeogr. Palaeoclimatol. Palaeoecol.* 312, 138–166.
- Herman, A.B., Domogatskaya, K.V., 2023. Ochotopteris—an Endemic Fern of the Mid-cretaceous Arctic. *Geosciences* 13, 279.
- Herranz, J.E., Pozo, M., 2022. Sepiolite and other authigenic mg-clay minerals formation in different palustrine environments (Madrid Basin, Spain). *Minerals* 12, 987.
- Hole, F.D., 1981. Effects of animals on soil. *Geoderma* 25, 75–112.
- Hovenden, M.J., Wills, K.E., Vander Schoor, J.K., Williams, A.L., Newton, P.C., 2008. Flowering phenology in a species-rich temperate grassland is sensitive to warming but not elevated CO<sub>2</sub>. *New Phytol.* 178 (4), 815–822.
- Huang, C.M., Retallack, G.J., Wang, C.S., 2012. Early Cretaceous atmospheric pCO<sub>2</sub> levels recorded from pedogenic carbonates in China. *Cretaceous Res.* 33 (1), 42–49.
- Hunter, S.J., Valdes, P.J., Haywood, A.M., Markwick, P.J., 2008. Modelling Maastrichtian climate: investigating the role of geography, atmospheric CO<sub>2</sub> and vegetation. *Clim. Past Discuss.* 4 (4), 981–1019.
- Iacoviello, F., Giorgetti, G., Nieto, F., Memmi, I.T., 2012. Evolution with depth from detrital to authigenic smectites in sediments from AND-2A drill core (McMurdo Sound, Antarctica). *Clay Miner.* 47 (4), 481–498.
- Isbell, R.F., 2021. National Committee on Soil and Terrain. *The Australian Soil Classification*, 3rd ed vol. 4. CSIRO Publishing, Melbourne.
- Jenny, H., 1941. *Factors of Soil Formation: A System of Quantitative Pedology*. McGraw-Hill, New York.
- Joeckel, R.M., Ludvigson, G.A., Kirkland, J.I., 2017. Lower cretaceous paleo-Vertisols and sedimentary interrelationships in stacked alluvial sequences, Utah, USA. *Sediment. Geol.* 361, 1–24.
- Kast, S., Rogers, R., Rogers, K.C., 2008. Reconstructing late cretaceous climate in the Mahajanga Basin of northwestern Madagascar. *J. Vertebr. Paleontol.* 28, 99.
- Keighley, D.G., Pickerill, R.K., 1994. Flute-like marks and associated structures from the Carboniferous Port Hood Formation of Eastern Canada; evidence of secondary origin in association with sediment intrusion. *J. Sediment. Res.* 64 (2a), 253–263.
- Kellner, A.W., Weinschütz, L.C., Holgado, B., Bantim, R.A., Sayao, J.M., 2019. A new toothless pterosaur (Pterodactyloidea) from Southern Brazil with insights into the paleoecology of a cretaceous desert. *An. Acad. Bras. Cienc.* 91 (Suppl. 2), e20190768.
- Khormali, F., Abtahi, A., 2003. Origin and distribution of clay minerals in calcareous arid and semi-arid soils of Fars Province, southern Iran. *Clay Miner.* 38, 511–527.
- Kidder, D.L., Worsley, T.R., 2012. A human-induced hothouse climate. *GSA Today* 22 (2), 4–11.
- Kishné, A.S., Morgan, C.L.S., Miller, W.L., 2009. Vertisol crack extent associated with gilgai and soil moisture in the Texas Gulf Coast Prairie. *Soil Sci. Soc. Am. J.* 73 (4), 1221–1230.
- Kraus, M.J., 1999. Paleosols in clastic sedimentary rocks: their geologic applications. *Earth Sci. Rev.* 47, 41–70.
- Kraus, M.J., Hasiotis, S.T., 2006. Significance of different modes of rhizolith preservation to interpreting paleoenvironmental and paleohydrologic settings: examples from Paleogene paleosols, Bighorn Basin, Wyoming, USA. *J. Sediment. Res.* 76, 633–646.
- Kumar, A., Singh, S., Khosla, A., 2021. Palaeosols and paleoclimate reconstruction of the Maastrichtian Lameta formation, Central India. *Cretac. Res.* 117, 104632.
- Ladeira, F.S.B., Mescalotti, P.C., Pupim, F.N., Faria, L.M.D.M., Assine, M.L., 2022. Paleosols record dry and humid paleoenvironments during the Upper Pleistocene in the Brazilian Pantanal. *Catena* 212, 106113.
- Laming, D.J.C., 1970. New Red Sandstone of Tor Bay, Petitor and Shaldon. *Rep. Trans. Devon. Assoc. Adv. Sci.* 101, 207.
- Lang, R., 1920. *Verwitterung und Bodenbildung als Einführung in die Bodenkunde*. Schweizerbart Science Publishers, Stuttgart.
- Lavelle, P., Spain, A.V., 2001. Soil organisms. *Soil Ecol.* 201–356.
- Lizzoli, S., Varela, A.N., Raigemborn, M.S., Richiano, S.M., Santamarina, P., Loinaze, V.S., 2024. Reconstruction of a deep-time critical zone in southern Patagonia (mid-high paleolatitude) during the mid-cretaceous greenhouse. *Catena* 241, 108054.
- Lizzoli, S., Raigemborn, M.S., Varela, A.N., Paredes, J.M., 2025. Paleosols as paleoclimate proxies to reconstruct mid-cretaceous paleoclimate conditions in Central Patagonia, Argentina. *Sediment. Geol.* 478, 106836.
- Martinelli, A.G., Riff, D., Lopes, R.P., 2011. Discussion about the occurrence of the genus *Aeolosaurus* Powell 1987 (Dinosauria, Titanosauria) in the Upper cretaceous of Brazil. *Gaea: J. Geosci.* 7, 34.
- Menezes, M.N., Dal'Bó, P.F.F., Smith, J.J., Rodrigues, A.G., 2021. The influence of ancient soil biota on the precipitation and distribution of pedogenic carbonate in paleosols of the Marília Formation (Upper cretaceous, Brazil). *Palaeogeogr. Palaeoclimatol. Palaeoecol.* 571, 110375.
- Menezes, M.N., Dal'Bó, P.F.F., Smith, J.J., Rodrigues, A.G., Rodrigues-Berrigue, A., 2022. Maastrichtian atmospheric pCO<sub>2</sub> and climatic reconstruction from carbonate paleosols of the Marília Formation (Southeastern Brazil). *J. Sediment. Res.* 92, 775–796.
- Menezes, M.N., Dal'Bó, P.F.F., Smith, J.J., Borghi, L., Arena, M., Favoreto, J., Araújo-Júnior, H.I., 2024. Pedogenic processes and climatic conditions from cretaceous (Albian) tropical paleosols of the Itapecuru Formation, Parnaíba Basin, Northeast Brazil. *Palaeogeogr. Palaeoclimatol. Palaeoecol.* 633, 111881.
- Meunier, A., 2005. *Clays*. Springer, Berlin, p. 472.
- Mineiro, A.S., Santucci, R.M., 2018. Ichnofabrics and ichnofossils from the continental deposits of the Serra da Galga Member, Marília Formation, Bauru Group (Upper cretaceous), Uberaba, Minas Gerais, Brazil. *J. S. Am. Earth Sci.* 86, 287–300.

- Mora, C.I., Sheldon, B.T., Elliott, W.C., Driese, S.G., 1998. An oxygen isotope study of illite and calcite in three Appalachian Paleozoic vertic paleosols. *J. Sediment. Res.* 68, 456–464.
- Müller, A.H., 1975. Zur Ichnologie limnische terrestrischer Sedimentations-rafime mit Bemerkungen fiber Ichnia landbewohnender Arthropoden aus Gegenwart und geologischer Vergangenheit. *Frieburg. Forschungsh.* C304, 79–87.
- Nascimento, D.L., Batezelli, A., Ladeira, F.S.B., 2019. The paleoecological and paleoenvironmental importance of root traces: Plant distribution and topographic significance of root patterns in Upper Cretaceous paleosols. *Catena* 172, 789–806.
- Nascimento, D.L., Netto, R.G., 2019. *Skolithos serratus* in paleosols: paleobiological, paleoecological, and paleobiogeographical insights. *Palaeogeogr. Palaeoclimatol. Palaeoecol.* 530, 152–162.
- Nascimento, D.L., Netto, R.G., Batezelli, A., Ladeira, F.S.B., Sedorko, D., 2022. Taenidium barretti ichnofabric and rainfall seasonality: Insights into dryland suites of Scovienia ichnofacies. *J. Palaeogeogr.* <https://doi.org/10.1016/j.jop.2022.10.001>.
- Nettleton, W.D., Price, A.B., Bowman, G.A., 1990. Argillitic horizon formation in late Wisconsinan eolian materials in Southwest Colorado, USA. In: *Developments in Soil Science*, vol. 19. Elsevier, pp. 149–154.
- Netto, R.G., 2007. Skolithos-Dominated Piperock in Nonmarine Environments: An Example from the Triassic Caturrita Formation, southern Brazil.
- Nordt, L., Atchley, S., Dworkin, S., 2003. Terrestrial evidence for two greenhouse events in the latest Cretaceous. *GSA today* 13 (12), 4.
- Nordt, L.C., Boutton, T.W., Jacob, J.S., Mandel, R.D., 2002. C4 plant productivity and climate-CO<sub>2</sub> variations in south-central Texas during the late Quaternary. *Quat. Res.* 58 (2), 182–188.
- Nordt, L.C., Driese, S.G., 2010. A modern soil characterization approach to reconstructing physical and chemical properties of paleo-Vertisols. *Am. J. Sci.* 310, 37–64.
- Ohba, M., Samonds, K.E., LaFleur, M., Ali, J.R., Godfrey, L.R., 2016. Madagascar's climate at the K/P boundary and its impact on the island's biotic suite. *Palaeogeogr. Palaeoclimatol. Palaeoecol.* 441, 688–695.
- Pal, D.K., Bhattacharya, T., Chandran, P., Ray, S.K., Satyavathi, P.L.A., Durge, S.L., Maurya, U.K., 2009. Vertisols (cracking clay soils) in a climosequence of Peninsular India: evidence for Holocene climate changes. *Quat. Int.* 209 (1–2), 6–21.
- Pearson, N.J., Gingras, M.K., 2006. An ichnological and sedimentological facies model for muddy point-bar deposits. *J. Sediment. Res.* 76, 771–782.
- Pierre, T.J., Primus, A.T., Simon, B.D., Philemon, Z.O.Z., Hamadjida, G., Monique, A., Lucien, B.D., 2019. Characteristics, classification and genesis of vertisols under seasonally contrasted climate in the Lake Chad Basin, Central Africa. *J. Afr. Earth Sci.* 150, 176–193.
- Probert, M.E., Fergus, I.F., Bridge, B.J., McGarry, D., Thompson, C.H., Russell, J.S., 1987. *The Properties and Management of Vertisols*, p. 36.
- Prochnow, S.J., Nordt, L.C., Atchley, S.C., Hudec, M.R., 2006. Multi-proxy paleosol evidence for middle and late Triassic climate trends in eastern Utah. *Palaeogeogr. Palaeoclimatol. Palaeoecol.* 232, 53–72.
- Quan, C., Han, S., Uttescher, T., Zhang, C., Liu, Y.S.C., 2013. Validation of temperature–precipitation based aridity index: Paleoclimatic implications. *Palaeogeogr. Palaeoclimatol. Palaeoecol.* 386, 86–95.
- Raiemborn, M.S., Lizzoli, S., Moyano-Paz, D., Varela, A.N., Poiré, D.G., Loinaze, V.S.P., Vera, E.I., Manabe, M., Tsuihji, T., Sano, T., Novas, F.E., 2025. Maastrichtian climate of southern Patagonia (Argentina): an approach from paleosols of the dinosaur-bearing Chorrillo Formation. *Cretac. Res.* 174, 106144.
- Ratcliffe, B.C., Fagerstrom, J.A., 1980. Invertebrate lebensspuren of Holocene floodplains: their morphology, origin and paleoecological significance. *J. Paleontol.* 614–630.
- Reineck, H.E., 1963. Sedimentengefüge im Bereich der südlichen Nordsee. *Abh. Senckenb. Naturforsch. Ges.* 505, 1–138.
- Retallack, G.J., 1990. Soils of the Past: An Introduction to Paleopedology. Unwin Hyman, London, p. 520.
- Retallack, G.J., 1997. Early forest soils and their role in Devonian global change. *Science* 276, 583–585.
- Retallack, G.J., 2001. Soils of the Past: An Introduction to Paleopedology. Blackwell, Oxford.
- Riccomini, C., Sant'Anna, L.G., Ferrari, A.L., 2004. Geologia do Continente Sul-Americano: Evolução da Obra de Fernando Flávio Marques de Almeida: São Paulo, Beca, 383–405. Evolução geológica do rift continental do sudeste do Brasil.
- Rodrigues, A.G., Dal'Bó, P.F., Basilici, G., Soares, M.V.T., Menezes, M.N., 2019. Biotic influence in the genesis of laminar calcretes in Vertisols of the Marília Formation (Upper cretaceous, Brasil). *J. Sediment. Res.* 89, 440–458.
- Rodríguez-Barreiro, I., Santos, A.A., Arribas, M.E., Mas, R., Arribas, J., Villanueva-Amadoz, U., Fernández-Baldo, F.T., Diez, J.B., 2022. The Jurassic–Cretaceous transition in the West Cameros Basin (Terra Group, Burgos, Spain): sedimentological and palynostratigraphical insights. *Cretac. Res.* 139, 105300.
- Rolle, W.D.I., 1980. Early invertebrate terrestrial faunas. In: Panchen, A.L. (Ed.), *The Terrestrial Environmental and the Origin of Land Vertebrates*, 15. *Syst. Assoc. Spec. Publ.*, pp. 117–157.
- Sa'eb, A.K., Taimeh, A.Y., 1998. Properties and characterization of Vertisols developed on limestone in a semi-arid environment. *J. Arid Environ.* 40 (3), 235–244.
- Santucci, R.M., Bertini, R.J., 2001. Distribuição paleogeográfica e biocronológica dos titanossauros (Saurischia, Sauropoda) do Grupo Bauru, Cretáceo Superior do sudeste brasileiro. *Revista Brasileira de Geociências* 31 (3), 307–314.
- Schellmann, W., 1981. Considerations on the definition and classification of laterites. In: *Lateritisation Processes. Proceedings of the International Seminar on Lateritisation Processes*, December 11–14, 1979, Trivandrum, India, pp. 1–10.
- Schlirf, M., Uchman, A., Kümmel, M., 2001. Upper Triassic (Keuper) non-marine trace fossils from the Haßberge area (Franconia, South-Eastern Germany). *Palz* 75, 71–96.
- Schoeneberger, P.J., Wysocki, D.A., Benham, E.C., 2012. *Field Book for Describing and Sampling Soils*. Government Printing Office.
- Sedorko, D., Alessandretti, L., Warren, L., Verde, M., Rangel, C.C., Ramos, K.S., Netto, R.G., 2020. Trace fossils from the Upper cretaceous Capacete Formation, Sanfranciscana Basin, Central Brazil. *Ann. Soc. Geol. Pol.* 90, 247–260.
- Sedorko, D., Melo, C.L., Ramos, R.R.C., Batezelli, A., Cambria, V., Goulart, V.R., Ramos, K.S., 2024. Ichnological analysis and paleoenvironmental inferences of Neogene meandering fluvial deposits in Continental Rift of Southeastern Brazil. *Brazil. J. Geol.* 54, e20230043.
- Sedorko, D., West, D.C., Nascimento, D.L., Mello, C.L., Ramos, R.R.C., Ramos, K.S., Scheffler, S.M., 2025. Trace fossil analysis in a Paleogene braided river system from the Volta Redonda Basin, Continental Rift of Southeastern Brazil. *Ichnos* 1–12 in press.
- Seilacher, A., 1964. Biogenic Sedimentary Structures. John Wiley & Sons, *Approaches to paleoecology*, Chichester, UK, pp. 296–316.
- Serrano, A.R., 1994. Os Cicindelídeos (Coleoptera: Cicindelidae): Taxonomia, Morfologia, Ontogenia, Ecologia e Evolução. Professor Germano, da Fonseca, Museu Bocage, Lisboa, pp. 233–285.
- Sheldon, N.D., Tabor, N.J., 2009. Quantitative paleoenvironmental and paleoclimatic reconstruction using paleosols. *Earth Sci. Rev.* 95, 1–52.
- Sheldon, N.D., Retallack, G.J., Tanaka, S., 2002. Geochemical clifomunctions from North American soils and application to paleosols across the Eocene–Oligocene boundary in Oregon. *J. Geol.* 110, 687–696.
- Silva, M.L., Batezelli, A., Ladeira, F.S.B., 2019. Genesis and evolution of paleosols of the Marília Formation, Maastrichtian of the Bauru Basin, Brazil. *Catena* 182, 1–28.
- Singh, A., Srivastava, A.K., 2021. Rhizosphere: a fascinating paleovegetational and paleoclimatic new intermediary in the Quaternary fluvio-lacustrine set-up of the Purna alluvial basin, Central India. *Rhizosphere* 20, 100430.
- Smith, J.J., Hasiotis, S.T., Kraus, M.J., Woody, D.T., 2008. Relationship of floodplain ichnocoenoses to paleopedology, paleohydrology, and paleoclimate in the Willwood Formation, Polecat Bench, Bighorn Basin, Wyoming, during the Paleocene-Eocene thermal Maximum. *PALAIOS* 23, 683–699.
- Smith, J.J., Platt, B.F., Ludvigson, G.A., Thomasson, J.R., 2011. Ant-nest ichnofossils in honeycomb calcretes, Neogene Ogallala Formation, High Plains region of western Kansas, U.S.A. *Palaeogeogr. Palaeoclimatol. Palaeoecol.* 308, 383–394.
- Soares, A.C.P., Seer, H.J., Moraes, L.C., 2017. Folha Uberaba - SE.23-Y-C-IV. Projeto triângulo mineiro – Companhia de Desenvolvimento de Minas Gerais (Codemge), escala 1:100.000.
- Soares, M.V.T., Basilici, G., Marinho, T.S., Martinelli, A.G., Marconato, A., Mountney, N.P., Colombera, L., Mesquita, Á.F., Vasques, J.T., Junior, F.R.A., Ribeiro, L.C.B., 2021. Sedimentology of a distributive fluvial system: the Serra da Galga Formation, a new lithostratigraphic unit (Upper cretaceous, Bauru Basin, Brazil). *Geol. J.* 56 (2), 951–975.
- Soil Survey Staff, 1999. *Soil Taxonomy. A Basic System of Soil Classification for Making and Interpreting Soil Surveys*. US Department of Agriculture, Natural Resource Conservation Service, Washington, DC.
- Soil Survey Staff, 2022. *Keys to Soil Taxonomy. A Basic System of Soil Classification for Making and Interpreting Soil Surveys*. U.S. Department of Agriculture/Natural Resources Conservation Service, p. 410.
- Stiles, C.A., Mora, C.I., Driese, S.G., Robinson, A.C., 2003. Distinguishing climate and time in the soil record: mass-balance trends in Vertisols from the Texas coastal prairie. *Geology* 31, 331–334.
- Stoops, G., Marcelino, V., Mees, F., 2010. *Interpretation of Micromorphological Features of Soil and Regoliths*. Elsevier Science, p. 752.
- Tabor, N.J., Myers, T.S., 2015. Paleosols as indicators of paleoenvironment and Paleoclimate. *Annu. Rev. Earth Planet. Sci.* 43, 11.1–11.29.
- Taheri, M., Khormali, F., Wang, X., Amini, A., Landi, A., Wei, H., Kehl, M., Chen, F., 2019. Clay mineralogy and geochemistry of the lower Pleistocene Loess in the Iranian Loess Plateau (Agh Band section) and implications for its provenance and paleoclimate change. *Quat. Int.* 552, 91–99.
- Thiede, D.S., Vasconcelos, P.M., 2010. Paraná flood basalts: rapid extrusion hypothesis confirmed by new 40Ar/39Ar results. *Geology* 38, 747–750.
- Trzciński, J., Wójcik, E., 2019. Application of microstructure classification for the assessment of the variability of geological-engineering and pore space properties in clay soils. *Open Geosci.* 11 (1), 236–248.
- Varela, A.N., Richiano, S.M., Poire, D.G., Iglesias, A., Brea, M., 2017. Characterization of a Heterogeneous Sequence Boundary Surface Perpendicular to the Patagonian Fold-and-Thrust Belt: The Role of Fossil Forest.
- Velde, B., 1995. *Origin and Mineralogy of Clays: Clays and the Environment. Compaction and Diagenesis*. Springer Berlin Heidelberg, Berlin, Heidelberg, pp. 220–246.
- Vepraskas, M.J., 2015. Redoximorphic features for identifying aquic conditions: North Carolina agricultural research service. *Tech. Bull.* 301.
- Vialov, O.S., 1962. *Problematika of the Beacon Sandstone at Beacon Hights, West Antarctica*. New Zealand J. Geol. Geophys. 5, 718–732.
- Wang, X., Wang, J., Xu, M., Zhang, W., Fan, T., Zhang, J., 2015. Carbon accumulation in arid croplands of Northwest China: pedogenic carbonate exceeding organic carbon. *Sci. Rep.* 5, 11439.
- Wilding, L.P., Williams, D., Miller, W., Cook, T., Eswaran, H., 1989. Close interval spatial variability of Vertisols: a case study in Texas. In: Proc. 6th Int. Soil Correlation meeting (VI ISCOM), Characterization, Classification and utilization of Cold Aridisols and Vertisols, pp. 232–247.
- Wilson, J.J., 1999. The origin and formation of clay minerals in soil: past, present, and future perspectives. *Clay Miner.* 34, 7–25.
- Wilson, M.D., Pittman, E.D., 1977. Authigenic clays in sandstones: recognition and influence on reservoir properties and paleoenvironmental analysis. *J. Sediment. Res.* 47 (1), 3–31.

- Wright, V.P., 1992. Paleopedology: Stratigraphic relationships and empirical models. In: Martini, I.P., Chesworth, W. (Eds.), Weathering, Soils and Paleosols. Developments in Earth Surface Processes, vol. 2, pp. 475–500.
- Wright, V.P., Platt, N.H., Marriott, S.B., Beck, V.H., 1995. A classification of rhizogenic (root-formed) calcretes, with examples from the Upper Jurassic-lower cretaceous of Spain and Upper cretaceous of Southern France. *Sediment. Geol.* 100, 143–158.
- Yaalon, D.H., Kalmar, D., 1978. Dynamics of cracking and swelling clay soils: Displacement of skeletal grains, optimum depth of slickensides, and rate of intra-pedonic turbation. *Earth Surface Proces.* 3, 31–42.
- Zalan, P.V., Oliveira, J.A.B.D., 2005. Origin and structural evolution of the Cenozoic Rift System of Southeastern Brazil; Origem e evolução estrutural do Sistema de Riftes Cenozoicos do Sudeste do Brasil. *Boletim de Geociências da Petrobras* 13.
- Köppen, W., 1923. Die Klimate der Erde. Walter de Gruyter & Co., Berlin und Leipzig.